SLAC-31
UC-28, Particle Accelerators
and High-Voltage Machines
UC-34, Physics
TID-4500 (31st Ed.)

ON THE THEORY OF IGNITRON BREAKDOWN IN MODULATOR SERVICE

July 1964

by

J. L. Cole and J. J. Muray

Technical Report
Prepared Under
Contract AT(04-3)-400
for the USAEC
San Francisco Operations Office

Printed in USA. Price $1.50. Available from the Office of Technical Services, Department of Commerce, Washington 25, D.C.

ACKNOWLEDGMENT

The authors wish to thank Dr. M. Sands and Dr. K. H. Kingdon for their helpful discussions. They are thankful to Mr. H. C. Steiner and Mr. J. L. Zehner of General Electric Company, and to Mr. D. E. Marshall of Westinghouse Electric Corporation for their advice and valuable discussions.

This experiment would not have been possible without the full cooperation of the modulator operator and design technician, Armin Wolff.

The authors are indebted to Mr. John Ferguson and Mr. Ivan Lutz for their helpful criticism and advice.

TABLE OF CONTENTS

LIST OF FIGURES

I. CIRCUIT DESCRIPTION

The 25 GeV electron beam of the Stanford two-mile linear accelerator will be deflected by a beam switching magnet to different target areas on a pulse-to-pulse basis. The purpose of this report is to give an account of the observed ignitron breakdown processes in the pulser of the beam switching magnet and to provide some theoretical explanations of these breakdown mechanisms.

The pulsed magnet to be used actually consists of five one-meter sections and is to be powered by ten high voltage (5 kV) modulators. Each of the five magnets is excited with two pulsers; separate pulsers are required for pulsing the beam left and right because the beams going to different target areas will have different energies. The magnetic field should be continuously variable to accommodate any beam energy. The pulser will run at any repetition rate up to 360 pulses per second and will produce a sinusoidal current pulse with a peak value that provides 2400 gauss in the magnet.

The current in the prototype modulator is switched by ignitrons. In order to reach the peak magnetic field in the magnet, 125 joules should be stored in the field. If the energy is dissipated after each pulse, the average power wasted would be 225 kilowatts for the whole deflection system. This amount of power is not only an expensive waste, but would require a large cooling system to remove the heat. It is therefore desirable to have a modulator that can recover as much of the energy as possible from the magnet and store it to be used for the next pulse. The modulator should be able to pulse the magnet with an accuracy of 1% in field value, and be ready to repeat the operation in less than 2.5 milliseconds.

The basic circuit for this prototype modulator is shown in Fig. 1 and the waveforms are shown in Fig. 2. The operation of the circuit can be given as follows: The storage capacitor (C1) is charged to +5 kV through ignitron V3. At time t_1, V1 is fired, causing the storage capacitor to discharge through the dummy coil. The current through L1 is one-half cycle of a 1000 cycle per second sine wave. The half-cycle of sine wave current flowing through C1 and L1 causes the voltage on C1

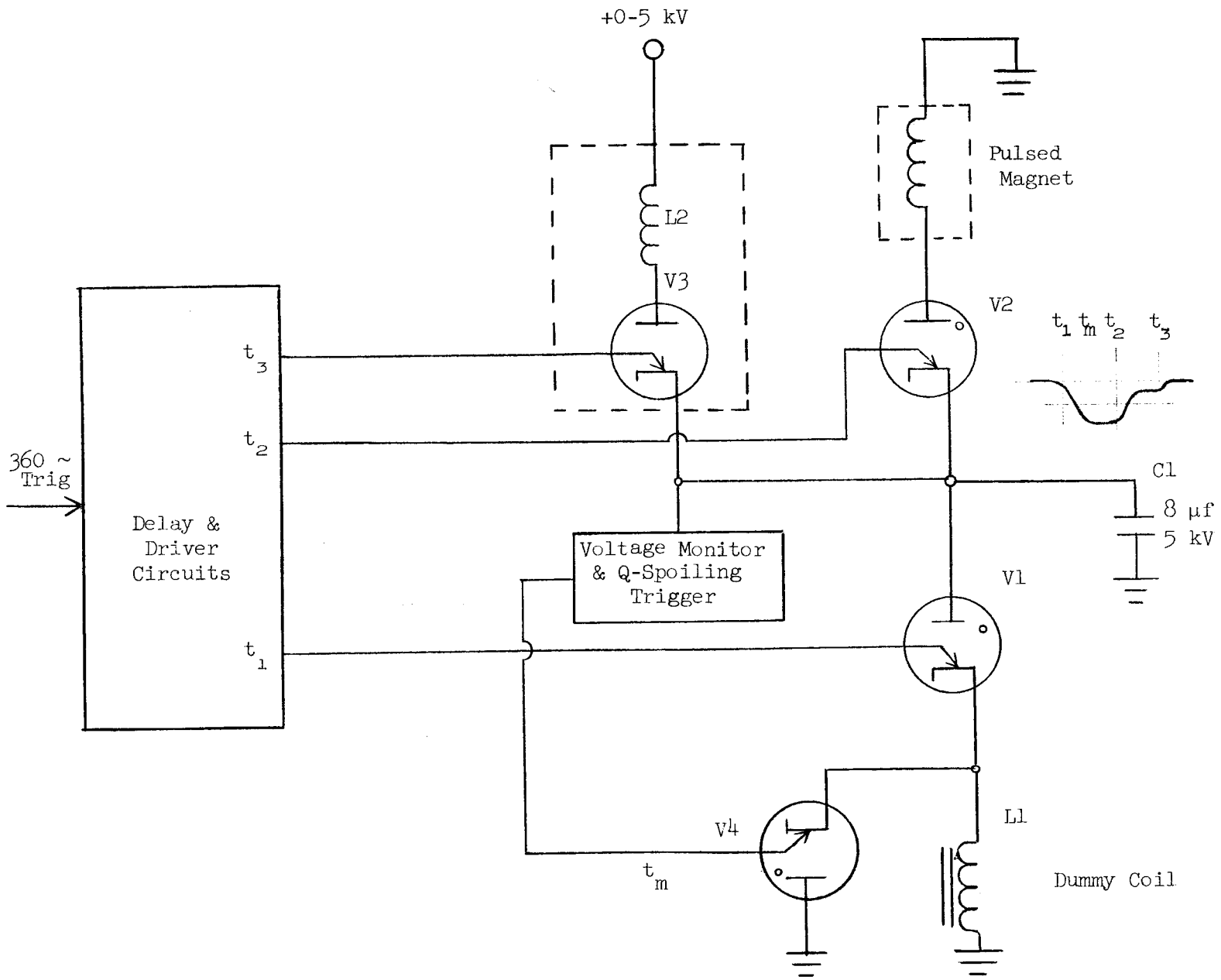

Fig. 1--Magnet pulser.

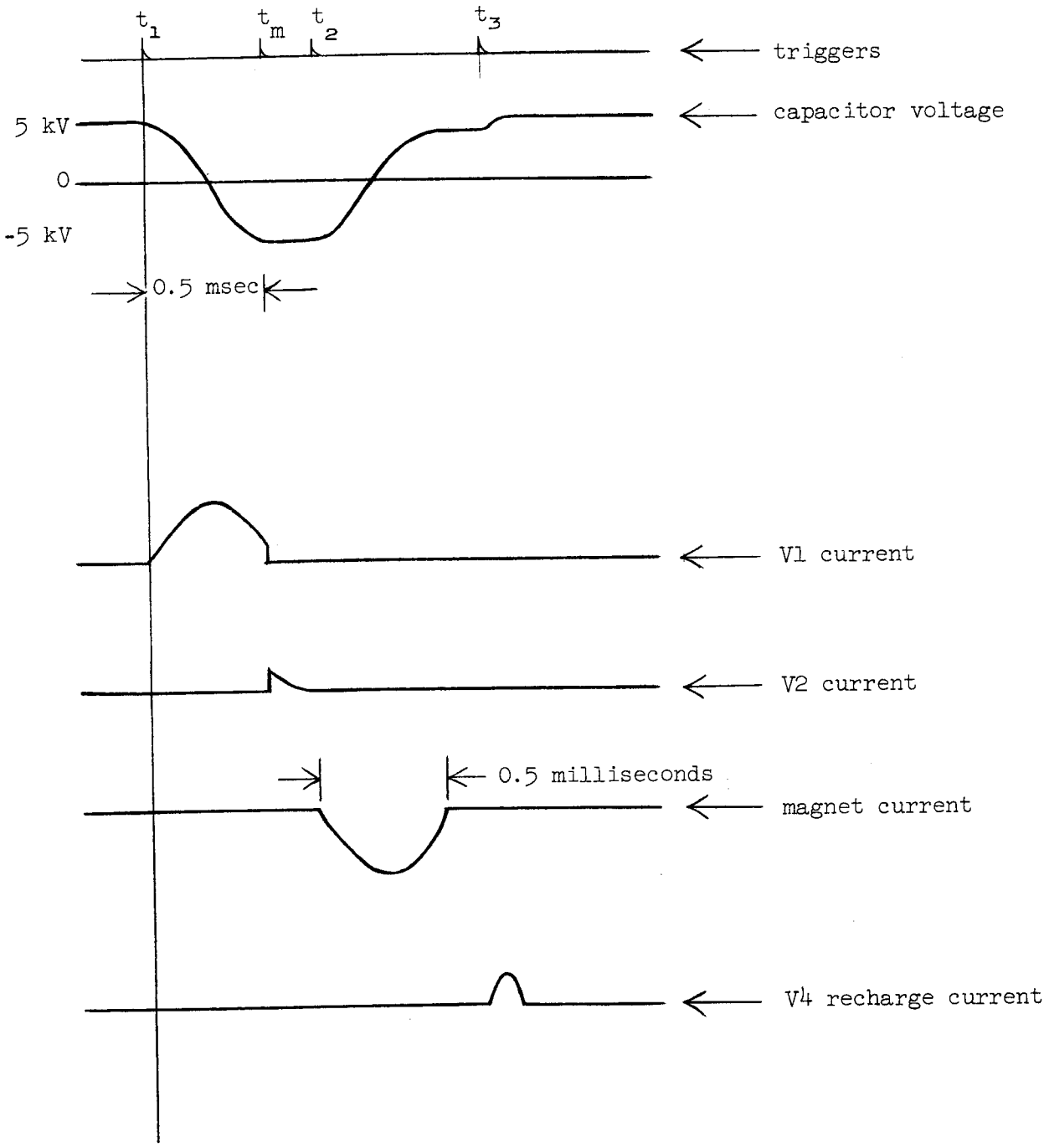

FIG. 2--Waveforms.

to reverse and approach -5 kV. As this voltage approaches -5 kV, it is monitored by the monitor circuit; when it reaches a specified level, a trigger pulse is produced that fires ignitron V4, which shorts out L1 and prevents C1 from being charged any higher. Therefore, a measured amount of energy ($1/2\ CV^2$) is stored in C1. This energy is now pulsed into the bending magnet by firing V2 at time t_2.

Firing V2 causes the polarity on C1 to reverse again, and C1 returns to approximately 80% to 90% of its original voltage (+5 kV). C1 is then recharged to 5 kV by firing V3 at time t_3. The cycle is now complete.

The magnet current, being a sine wave, is approximately flat at its peak during the time the 2-microsecond beam passes through the magnet. An amplitude error of 0.1% occurs at 2.5° of either side of the peak of the sine wave. Therefore, with a resonant frequency of 1000 cycles, the magnet current is flat to 0.1% for 14 microseconds. A similar calculation shows that 1.0% flatness can be obtained for $\pm 8.1^\circ$ or 44.8 microseconds.

Another source of error is the time jitter in the Q-spoiling trigger. Preliminary tests show that the error in the Q-spoiling circuit can be held to 0.1% if the line voltage variation is less than 5%.

During operation of the circuit, it was found that the ignitrons (V1 and V2) would break down when the pulser was operated simultaneously at full power and at full repetition rate, i.e., at 5kV, 160 amps, and 360 pulses per second. The types of ignitrons tried for V1 and V2 were WL5555, WL5552, and WL4681.

To understand why the ignitrons break down in this application, while in other circuits they have been used successfully to switch currents and voltages higher than those of this experiment, one must compare the circuits.

The magnet pulser consists of a switch in series with an RLC circuit. Thus it can be considered as a line type modulator with a one-section pulse line, in which case the losses in the circuit represent the resistive element, and the magnet is the inductance.

The inverse voltage on the switch tube is determined by the relative values of R_1, L_1, and C_1 and is given by the formula for the reflection

coefficient, Γ.

$$\Gamma = \frac{Z_R - Z_o}{Z_R + Z_o}$$

where $\Gamma = \frac{V_1}{V_o}$, Z_R = resistive losses in the circuit, and $Z_o = \sqrt{\frac{L}{C}}$.

The voltage across the capacitor before the ignitron fires is designated V_o, and V_1 is the capacitor voltage at the end of the energy recovery cycle. Then from

$$\Gamma = \frac{Z_R - Z_o}{Z_R + Z_o} = \frac{R - Z_o}{R + Z_o}$$

using $Z_o = \sqrt{\frac{L}{C}}$, $Q = \frac{\omega L}{R}$ and $\omega \approx \frac{1}{\sqrt{LC}}$ we obtain

$$Z_o = QR$$

and substituting QR for Z_o yields

$$\Gamma = \frac{R - QR}{R + QR} = \frac{1 - Q}{1 + Q} = (-1) + \left(\frac{2}{1 + Q}\right)$$

In the magnet pulser circuit the Q is high (50 to 100); therefore, the reflection coefficient (Γ) is approximately equal to -1.

The energy lost in one-half cycle is given by the equation

$$U_L = \tfrac{1}{2}C\left(V_o^2 - V_1^2\right)$$

or

$$U_L = \tfrac{1}{2}CV_o^2\left(1 - \Gamma^2\right)$$

Therefore, an efficient circuit is one with a large reflection coefficient ($\Gamma \approx -1$).

When ignitron V1 (Fig. 1) reaches the end of the first half-cycle, it stops conducting, and a large peak inverse voltage appears across it which is equal to the capacitor voltage. This is the result of the large reflection coefficient (Γ) which results from having a high Q circuit.

A. Klystron Modulator Service

In klystron modulator service, as shown in Fig. 3, the switch tube holds off the full capacitor voltage in the forward direction (anode positive) but is required to hold off only a small part of this voltage in the reverse direction.

B. Capacitor Discharge Service

Figure 4 diagrams the capacitor discharge service, in which the reflection coefficient (Q) is very high. The peak current is also very high, which causes a large amount of ionization to be present in the tube when the voltage tries to reverse. Because of the high degree of ionization, the tube cannot hold off the inverse voltage, and it therefore conducts in the reverse direction. This process continues for several cycles until most of the stored energy is dissipated. This type of breakdown cannot be tolerated in a high repetition pulser because of the time required for the circuit to recover.

C. Magnet Pulser

In the magnet pulsers shown in Fig. 5a and Fig. 5b, the reflection coefficient and the repetition rate are high. Therefore, the switch tube must be able to hold off both forward and reverse voltages, and no arc-overs can be tolerated.

The main difference between the one-coil system of Fig. 5a and the two-coil system of Fig. 5b is that in the one-coil system the second tube can be triggered at the time the first tube stops conducting, thereby removing the inverse voltage on the first tube. However, the second tube must still hold off the inverse voltage. One advantage of the two-coil system is that only half of the current flows through the magnet, thus reducing the heating problems. Another advantage is that

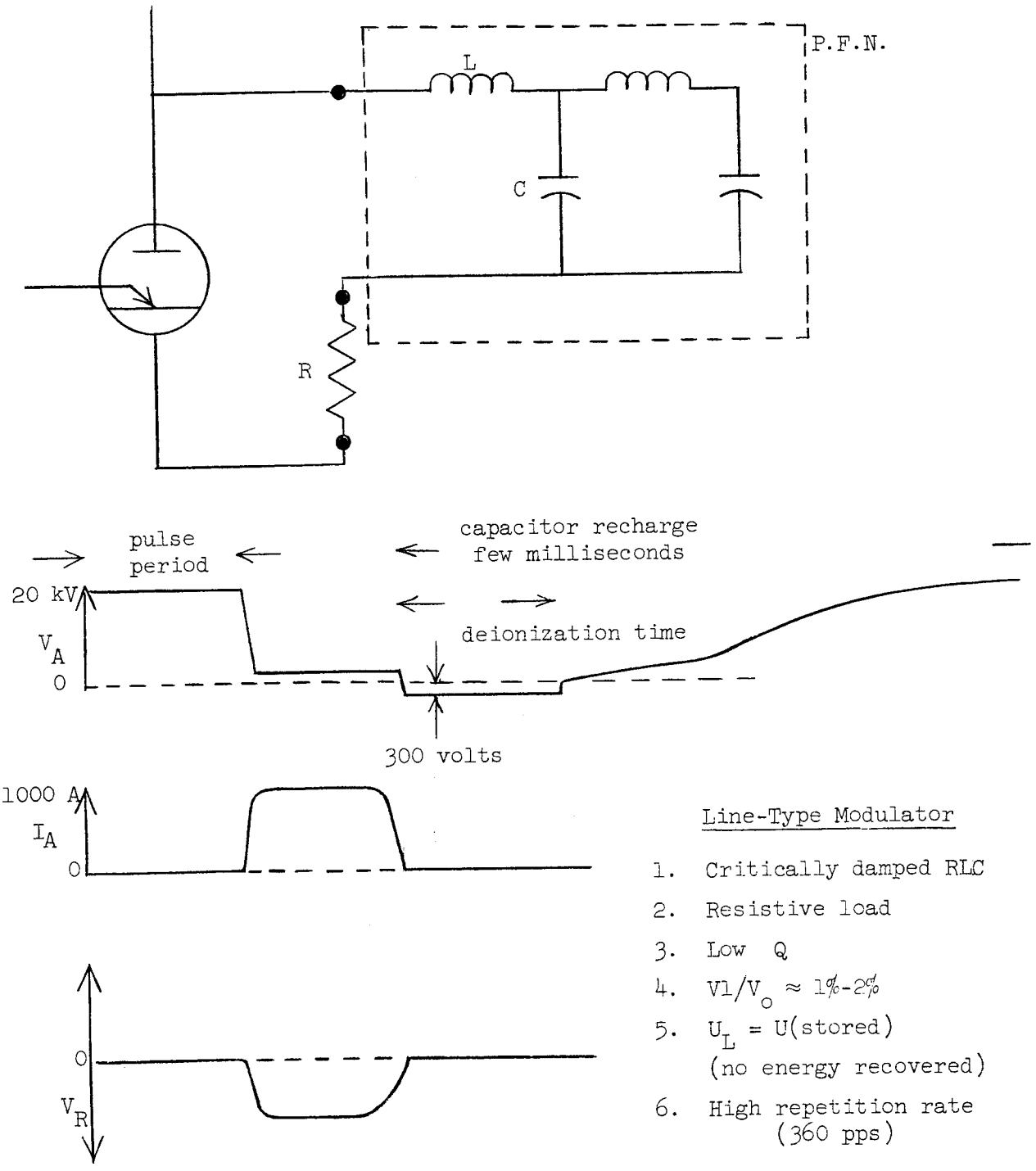

FIG. 3--Klystron line-type modulator.

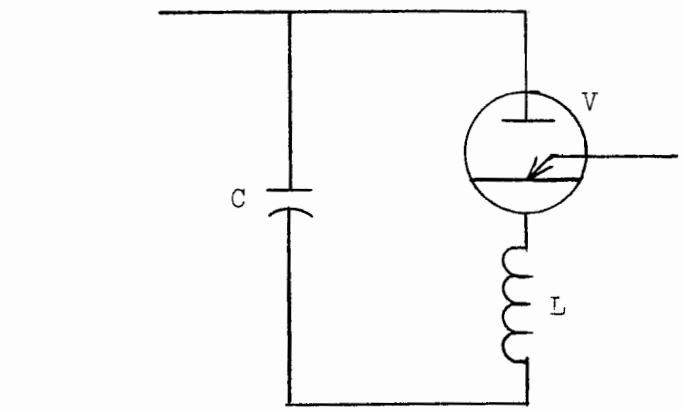

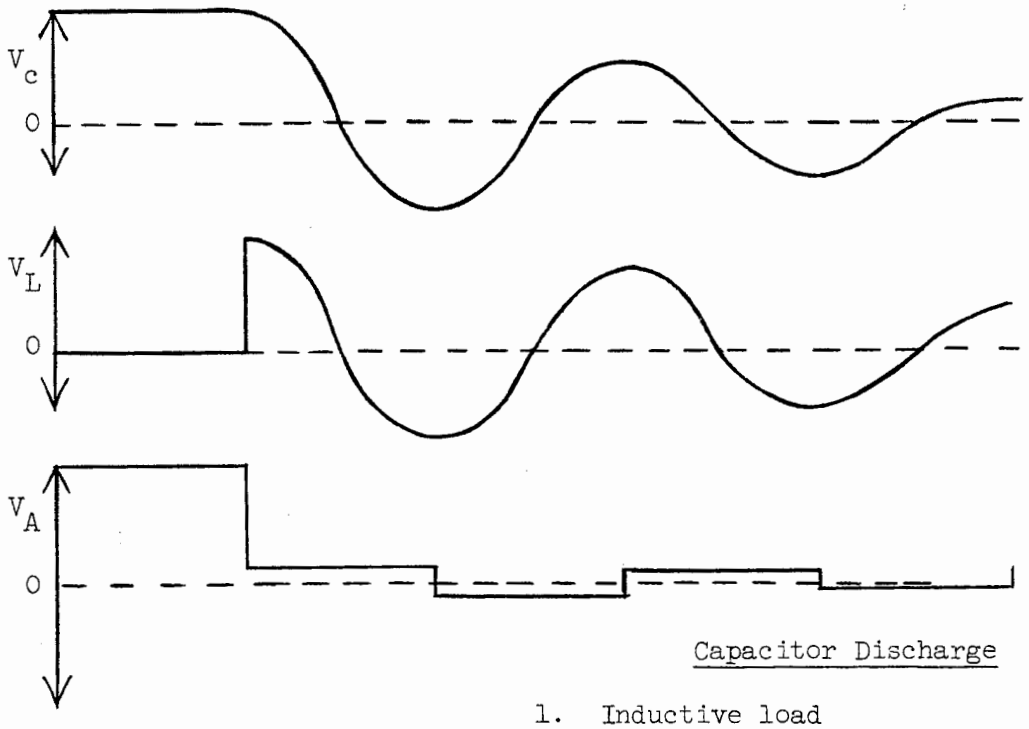

Capacitor Discharge

1. Inductive load
2. $U_L = U_{IN}$ (no power recovery)
3. Low repetition rate
4. Very high current (10^5 to 10^6 amps)

FIG. 4--Capacitor discharge circuit.

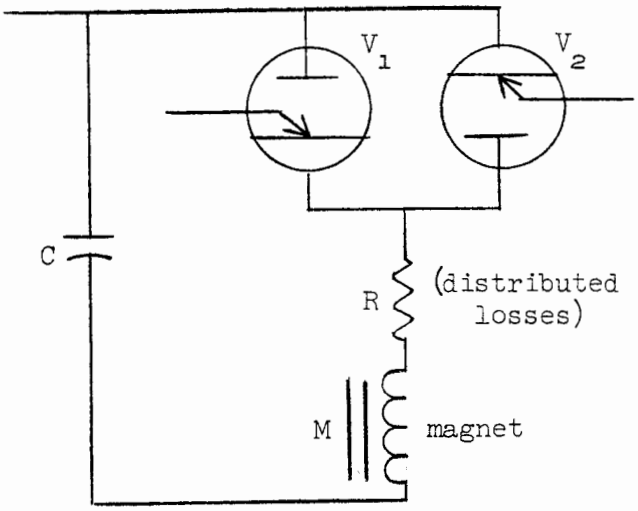

One-Coil System

1. Inductive load
2. High $Q \approx 50$ to 100
3. $U_L \leq U_{stored}$
4. $\frac{V_i}{V_o} \approx 90\%$
5. High repetition rate (360 pps)
6. Natural frequency $\omega \approx \frac{1}{\sqrt{LC}}$

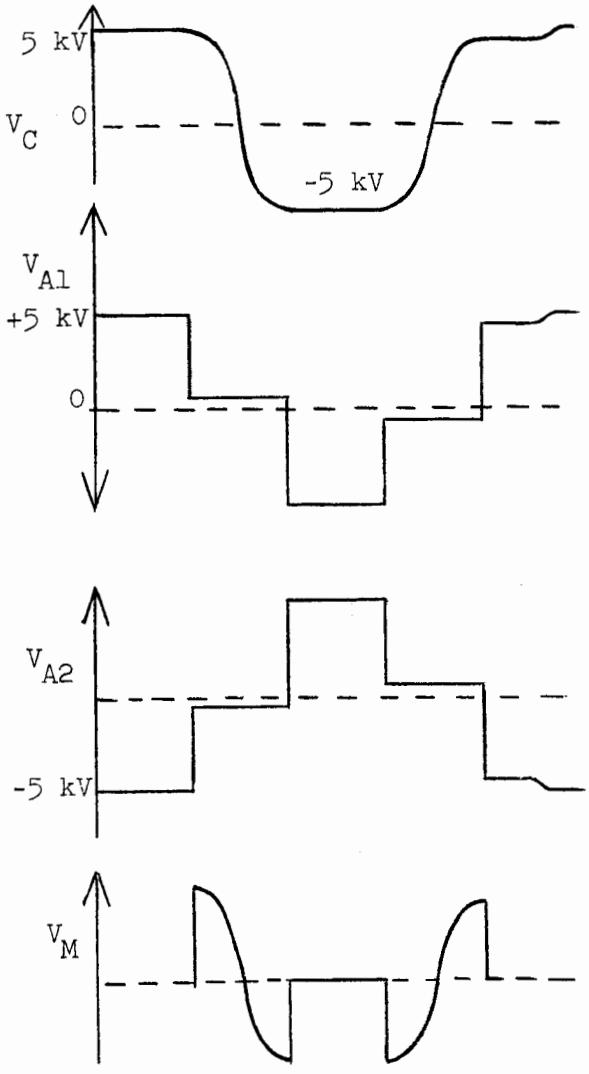

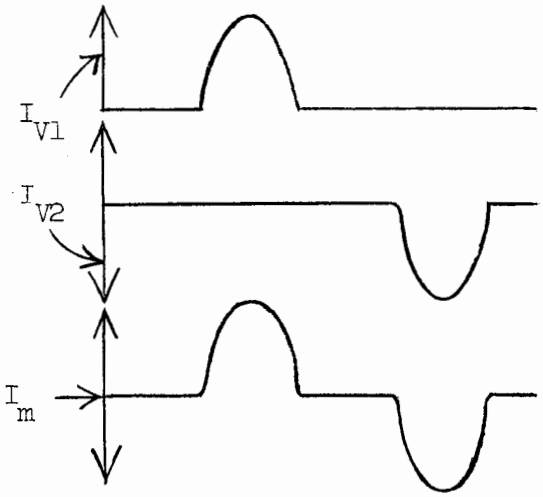

FIG. 5a--Magnet pulser: one-coil system.

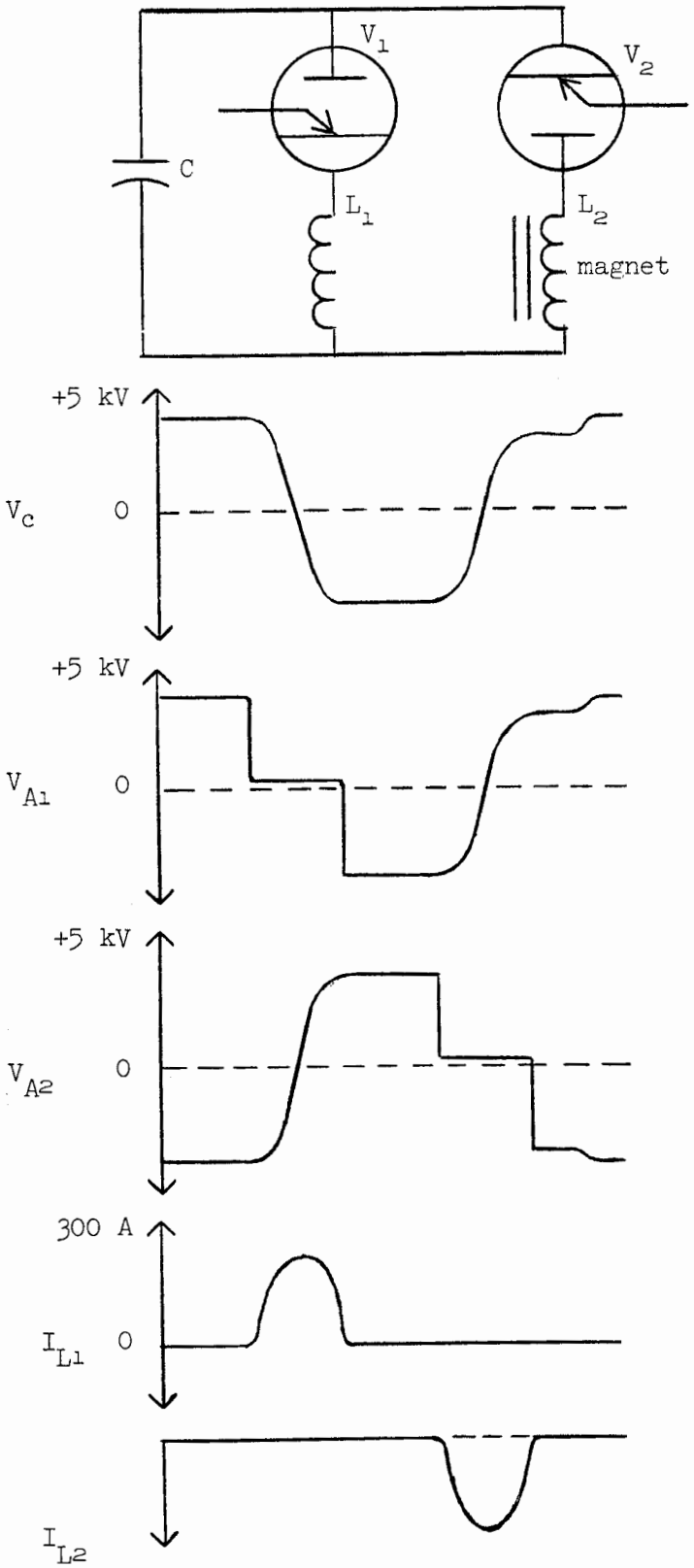

Two-Coil System

1. Inductive load
2. High $Q \approx 50$ to 100
3. $U_{loss} < U_{stored}$
4. $\frac{V_1}{V_o} \approx 90\%$
5. High repetition rate
6. $\omega = \frac{1}{\sqrt{LC}}$

Fig. 5b--Magnet pulser: two-coil system

only half of the current has to be transported from the pulser to the magnet, which improves the efficiency of the pulser because cable losses are lower.

II. VOLTAGE HOLD-OFF BEFORE PLASMA FORMATION

The ignitrons tested in the modulator circuit were single-anode gridless ignitrons constructed of stainless steel and sealed off. The important dimensions of the tubes used in the circuit are shown in Fig. 6. The basic difference between the two tubes is that one of them contains a baffle and ring (WL5555) to prevent the mercury droplets, ejected from the surface of the mercury, from hitting the anode during the conduction cycle. The effect of the baffle on the breakdown mechanism will be discussed later.

In this section we will consider the ignitron as a system of electrodes in mercury vapor, a long time after the last switching cycle. Under these conditions, the maximum hold-off voltage (breakdown voltage) between any two electrodes in mercury vapor is given by Paschen's law as a function of the product of the vapor pressure p and the gap between electrodes d. A typical pressure breakdown curve for static conditions in mercury is shown in Fig. 7. The vapor pressure p (in mm of mercury) may be represented, at temperature T, by

$$p = \exp\left(b - \frac{a}{kT}\right)$$

where a is the heat of evaporation of a molecule from the mercury surface, and b is a material constant. Figure 8 shows the dependence of the vapor pressure as a function of the equilibrium temperature. Generally, for ignitrons, the operating temperature and pressure are set by the temperature and the flow rate of the cooling water. However, dynamical effects can change the pressure condition, which will lower the breakdown voltage and can cause an arc-over in the tube. Under normal conditions, the breakdown voltage before the plasma formation is of the order of 40 to 80 kV at room temperature.

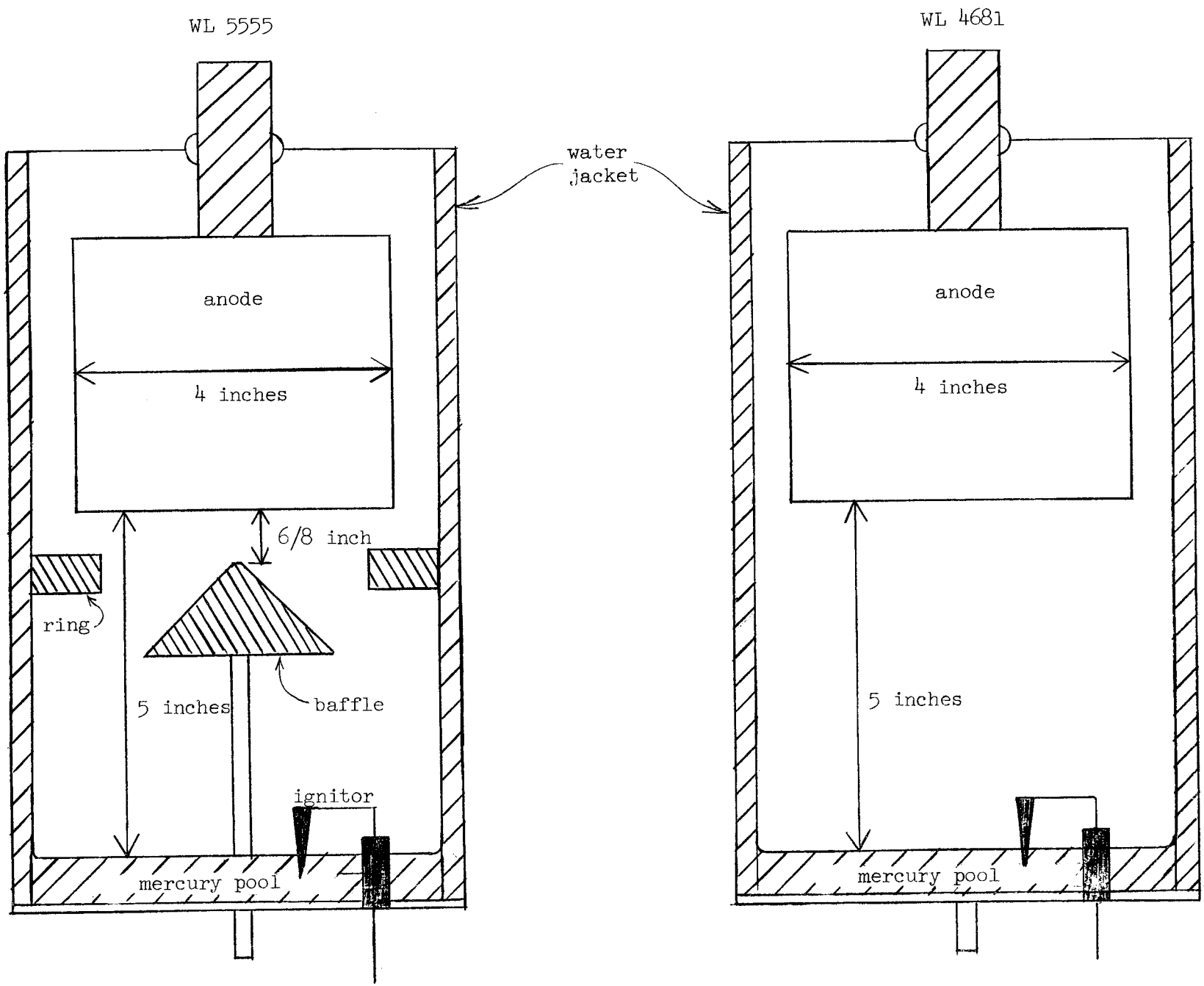

FIG. 6--Ignitrons tested in modulator circuit.

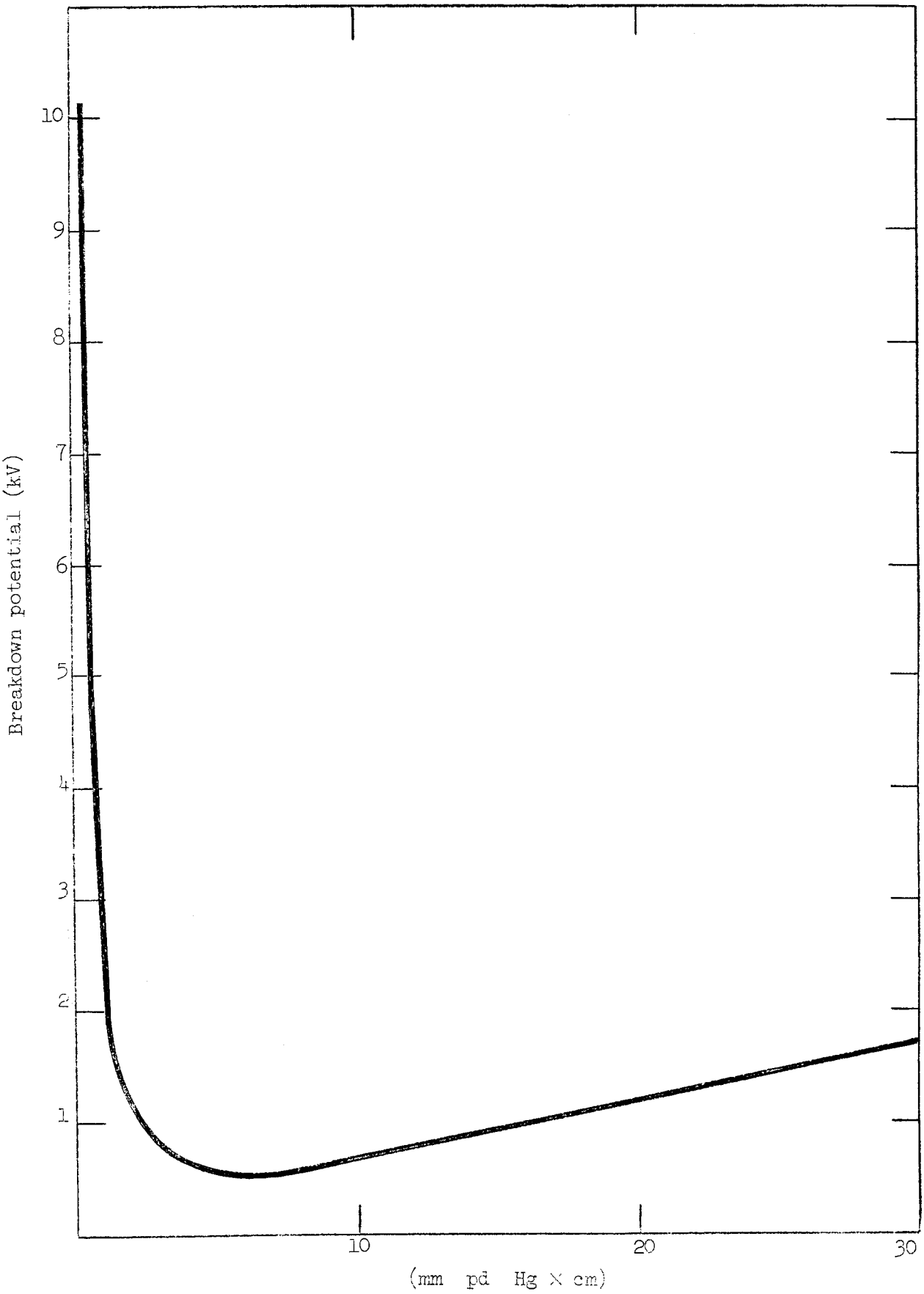

FIG. 7--Breakdown potential vs pd in mercury vapor.

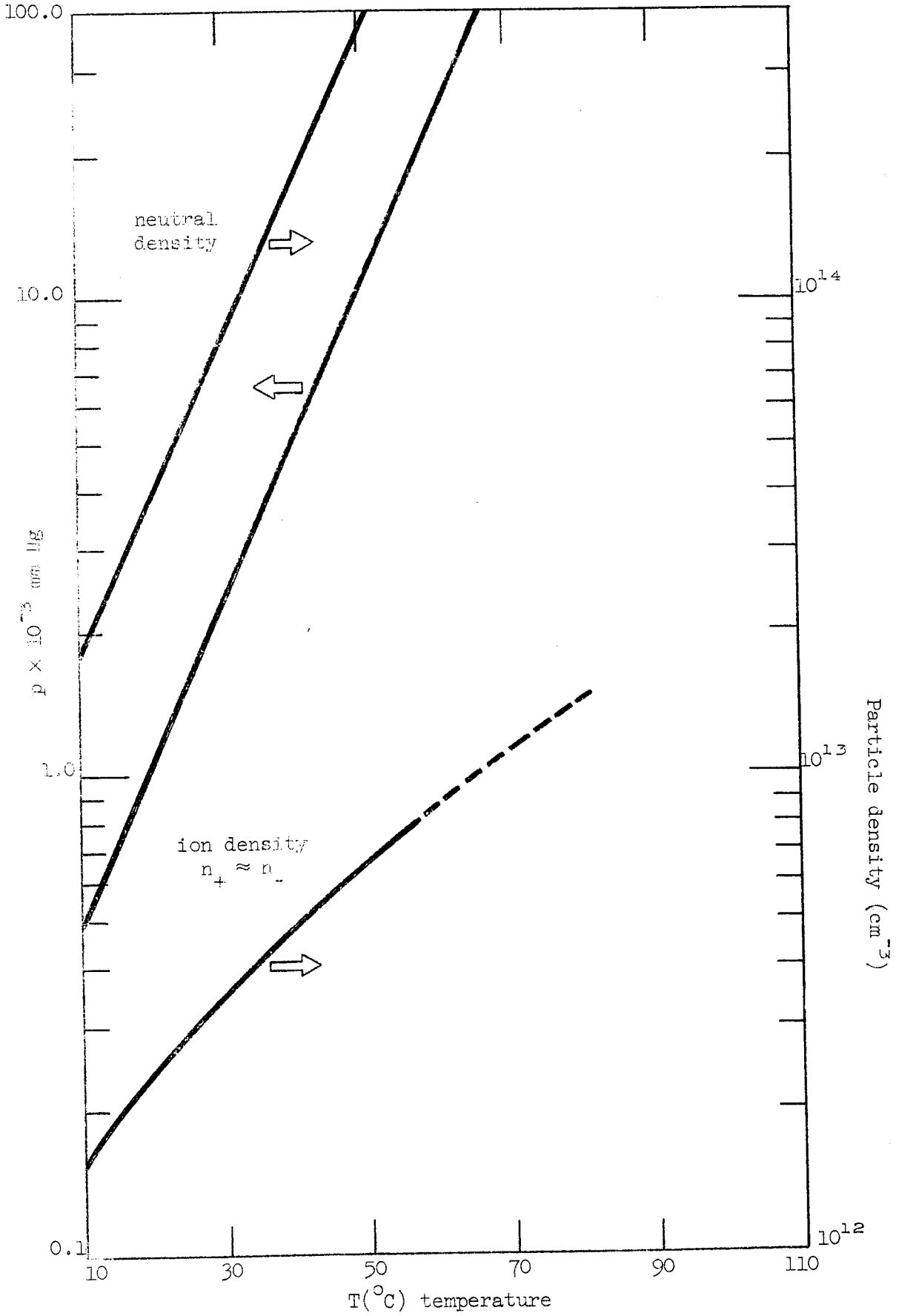

FIG. 8--Mercury vapor pressure as function of equilibrium temperature.

III. IGNITOR OPERATION

The ignitron conducts when current is passed through the ignitor into the mercury pool and the created charge carriers ionize the mercury vapor between the cathode and anode regions. Several physical theories have been proposed to explain arc ignition in mercury-pool tubes. Slepian suggested that the starting process might be caused by localized heating of the mercury, and the resulting higher vapor pressure would be favorable for arc and cathode spot formation.[1,2,3] Other authors[4,6] proposed that the high electric field applied to the mercury surface could initiate a spark discharge when the field emission current density reached a critical value corresponding to a field of 10^7 volts/cm. This value could be lower, 10^5 to 10^6 volts/cm, when there is a high current density passing through the micropoints on the mercury that are formed by the action of a strong electric field.[7] If the current density is high, the micropoints can be heated up and converted into a plasma state, which can be the main process for the generation of the charged particles.[5] The electrons leaving the ignitor can start an avalanche breakdown which makes the tube conduct.

The rate of formation of the mercury points depends on the intensity of the electric field and the amount of the initial surface deformation. According to Tonks,[7] the formation time for a micropoint is given by

$$t = \left[5.4 + 2.83 \ln\left(\frac{Y_o}{Y_a}\right)\right] / (E - E_c)^3$$

where t is in microseconds, the field E in megavolts/cm, and Y_a is the size of an initial micropoint in cm, referred to an arbitrary point Y_o. The critical field E_c = 57,000 volts/cm. The initial surface deformations may be due to thermal motions of the mercury, of amplitude

$$Y_a \approx \left[\frac{kT}{\gamma_o (1 - T/T_c)^{\frac{1}{2}}}\right]^{\frac{1}{2}}$$

where k is Boltzmann's constant, T is the absolute temperature, $\gamma_o \approx 470$ dyne/cm, the surface tension at $T = 0$, and $T_c = 1733^oK$ is the critical temperature at which the mercury surface vaporizes.

It was observed[6,8] that spark discharges in mercury are invariably accompanied by high velocity jets of mercury vapor and ejection of mercury droplets which travel at a velocity much slower than the accompanying pressure wave. The velocity of the vapor[6] depends on the current density, but it is of the order of 10^5 to 10^6 cm/sec. In this experiment the ions created by the ignitor were used to study the effect of the built-in obstacles, such as the baffle and the ring, on the ion migration. The simple circuit used for this experiment is shown in Fig. 9. The pressure in the tube was varied by changing the temperature of the cooling water for the tube. Typical photographs taken at constant ignitor power but at different temperatures are shown in Figs. 10a and 10b. The top trace shows the measured anode current as a function of the time for the tube which contains a baffle (5555); the next trace is the collected time dependent current for the other tube (4681), which does not have any obstacle between the mercury pool and the anode. It can be seen from the different form of the traces that the baffle both prevents the fast ion stream from arriving at the anode and decreases the magnitude of the positive ion current. This decrease in magnitude is probably explained by the increased diffusion loss to the wall.

The measured anode current dependence on the mercury pressure in the tube can be explained by assuming that the mercury ions are transported to the anode by the vapor stream of neutral mercury atoms and the process is governed by diffusion. The current I_A is then proportional to the transported charges per second, which is

$$I_A = jA = eD_+A\left(\frac{p_o}{p}\right)\frac{dn_+}{dx} \propto \frac{1}{p}$$

where A is the surface area of the anode and D_+ is the ion diffusion coefficient. The pressure dependence of the measured positive ion current is thus explained. If one measures the peak value of the current pulses as a function of the pressure, then the agreement with this

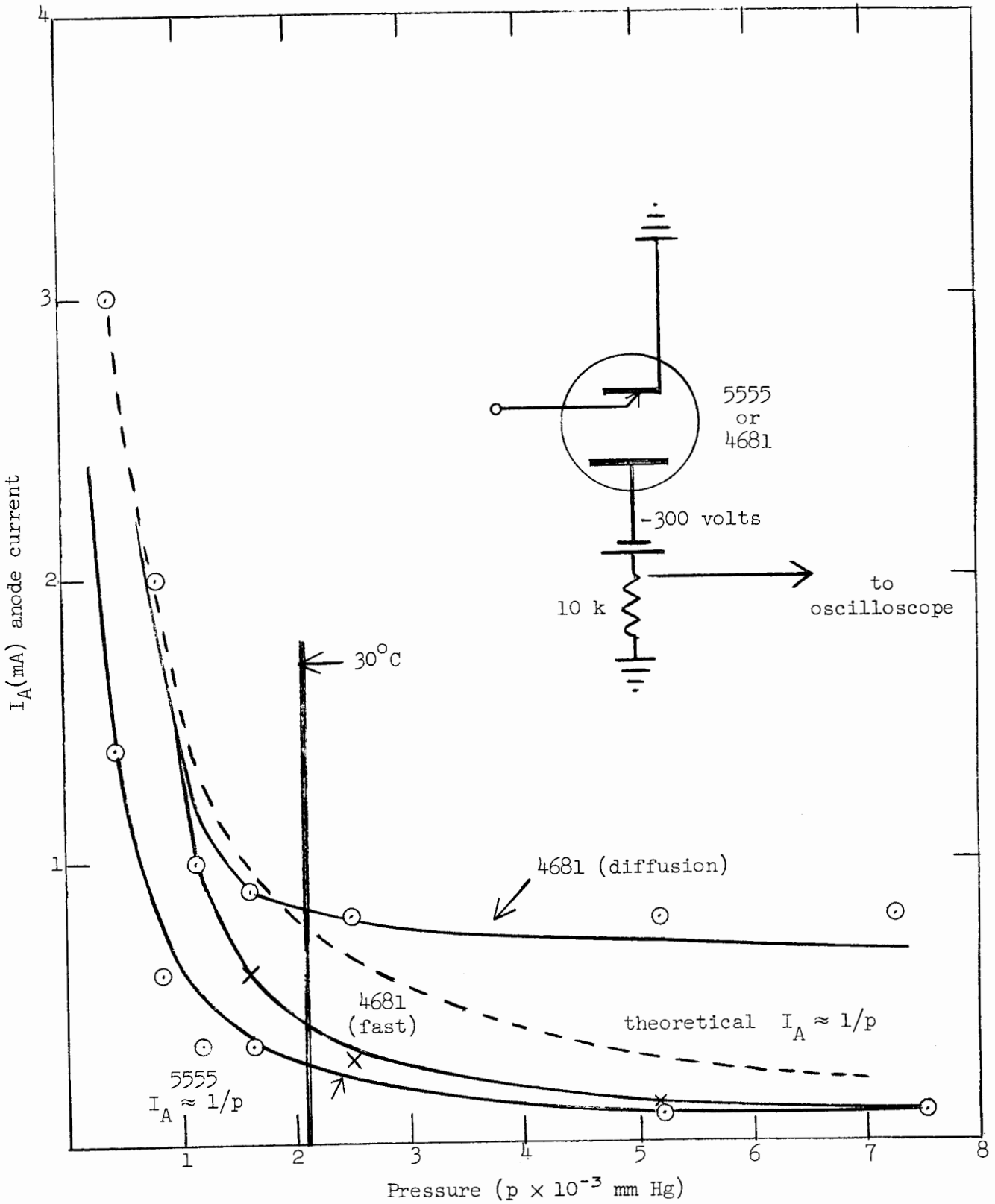

Fig. 9--Anode current vs pressure

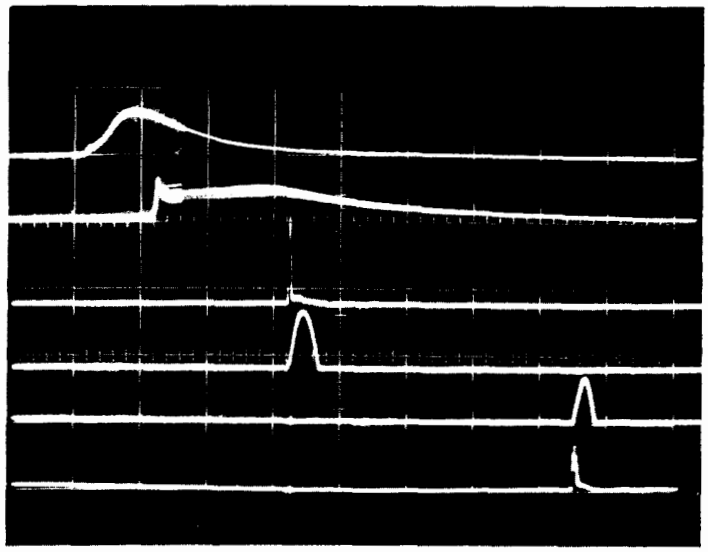

Fig. 10a--The two top lines represent the ion currents I_A (at $p = 4.2 \times 10^{-4}$ mm Hg and $T = 8^{\circ}C$) for the tubes 5555 and 4681, respectively, as a function of time. The sensitivities are 2 mA/cm and 5 mA/cm, and the horizontal sweep is 200 μsec/cm. The four traces below show the ignitor voltages (3rd and 6th trace) and the ignitor currents (4th and 5th trace) for the two tubes. (Sensitivity: 500 volts/cm, 100 amps/cm, and 50 μsec/cm.) The repetition rate is 60 pps.

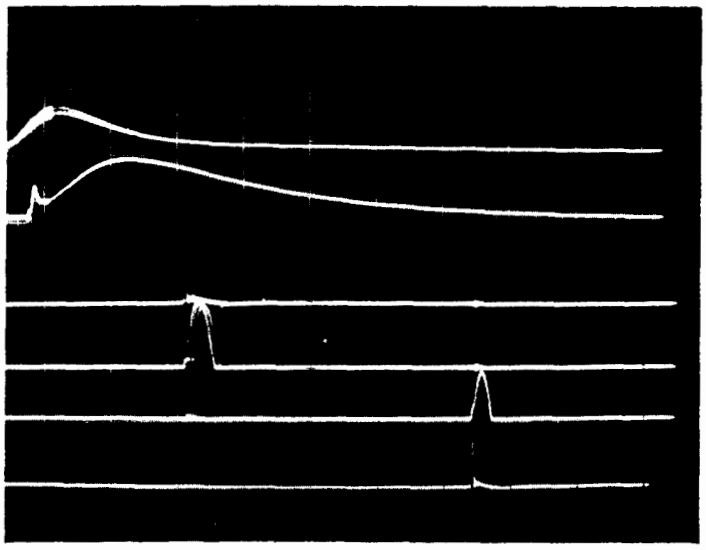

Fig. 10b--The two top lines represent the ion currents I_A (at $p = 1.6 \times 10^{-3}$ mm Hg and $T = 25^{\circ}C$ for the tubes 5555 and 4681. The sensitivities are 0.5 mA/cm and 1 mA/cm, respectively, and the horizontal speed is 500 μsec/cm. The ignitor voltages and current have the same sensitivity as in Fig. 10a.

Fig. 10--Wave forms of ion currents in ignitron with and without baffle.

prediction is very good for the 5555 tube (see Fig. 9). In this case only the diffusion current reaches the anode. However, for the 4681 tube one has to assume that the initial current density has two components, the convection part and the diffusion part; the total current density can then be written as

$$j_T = n_+ e v_+ + eD_+ \frac{dn_+}{dx} \frac{p_o}{p} = J(\text{fast}) + J(\text{diff})$$

The convection part decreases with increasing pressure whereas the diffusion part increases. This can explain the disagreement between the experimental values and the $I \approx 1/p$ curve shown in Fig. 9 for the case of the 4681 tube. It is worthwhile to note that because the ion migration can be influenced by spurious gases in the tube, this simple method can be used to measure spurious gas vapor pressures in mercury[9] or hydrogen tubes.

Figure 11 shows the measured pulse length as a function of the vapor pressure in the tube. If the tubes are operating at $T = 25^{\circ}C$, then the maximum repetition rate is approximately given by

$$\text{Repetition rate } (T = 25^{\circ}C) = \frac{1}{\text{pulse length}}$$

which is $R_{4681} \approx 235$ for the 4681 tube and $R_{5555} \approx 400$ for the 5555 tube. When the travel time of the neutral vapor streams is longer than the travel time of the ions, an even smaller value for the maximum repetition rate must be maintained if pressure build-up is to be prevented. It has been found experimentally, however, that the diffusion coefficient for ions is less than for neutral particles because of the possibility of cluster formation of molecules about an ion, which will result in increasing both the effective mass of the ion and its cross section. Other processes, such as the charge exchange

$$Hg^+(\text{fast}) + Hg(\text{slow}) \rightarrow Hg^+(\text{slow}) + Hg(\text{fast})$$

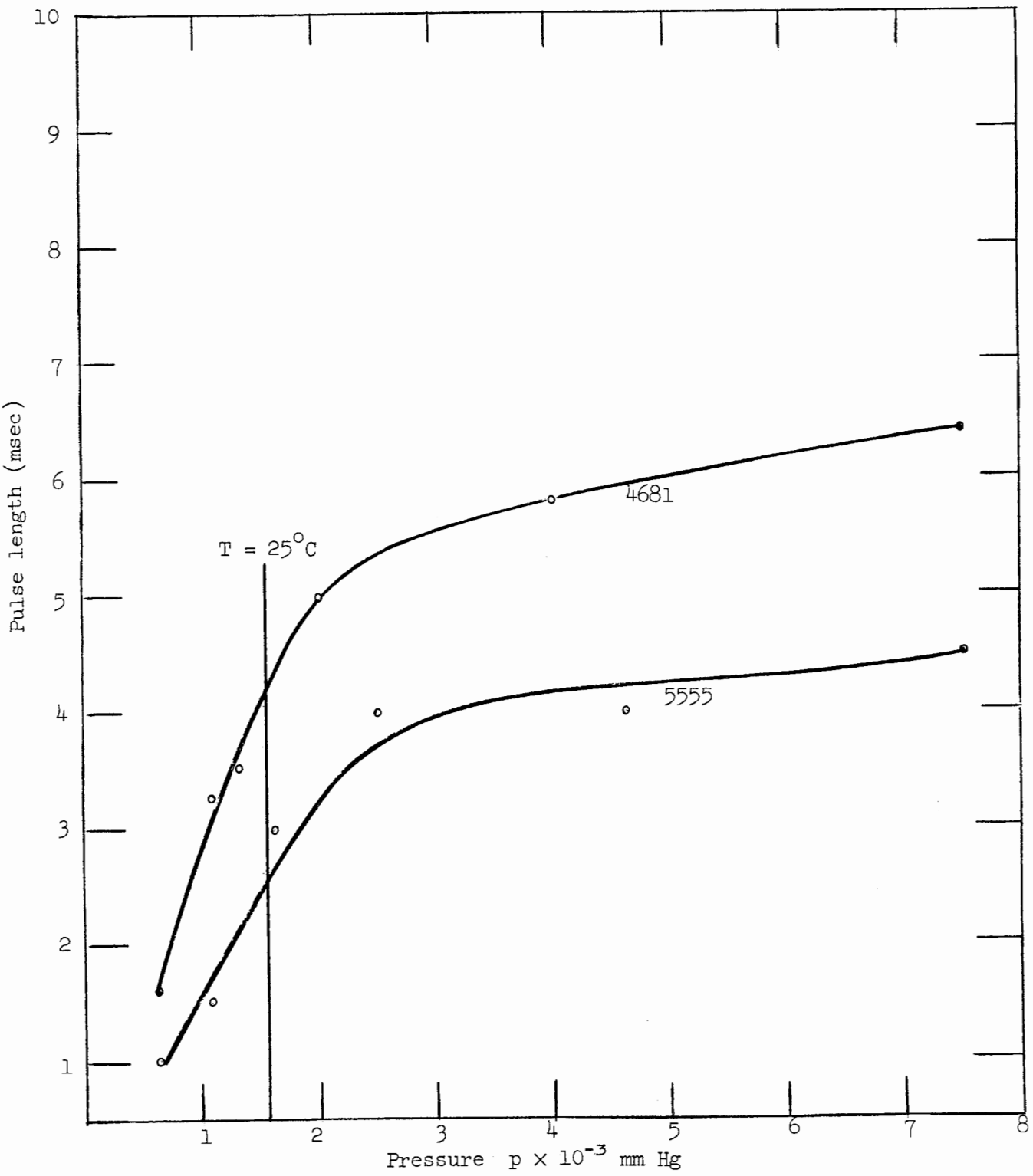

FIG. 11--Pulse length vs pressure.

can influence the ion diffusion, but the details are not known for this application. For calculation it will be assumed that

$$D_o \approx 5D_+$$

Figures 12a and 12b show the anode current waveforms at higher repetition rate (360 pps) for $T = 8^oC$ (Fig. 12a) and $T = 25^oC$ (Fig. 12b). The current build-up can be observed clearly in these pictures.

The main conclusion from this section is that it is possible to have a current (charge) and neutral (pressure) build-up between the cathode and anode regions either when the repetition rate or the operating temperature is high. In the next section the effect of this pressure build-up on the tube operation will be investigated.

IV. MECHANISM OF THE FORWARD BREAKDOWN

It was observed that ignitron V2 (Fig. 5a) broke down in the forward direction without firing the ignitor circuit when either the repetition rate or the temperature exceeded a certain value. With the 5555 tube no faults were observed for operation up to 180 pps at $T = 40^oC$, but this tube broke down continuously when triggered 360 times per second. The peak current was 160 amperes and the capacitor voltage was 5 kV. It was also observed that at higher temperatures the frequency of the forward breakdown increased and even at lower repetition rates it could easily be observed.

To investigate the mechanism of the forward breakdown, the simple test circuit shown in Fig. 13 was built. The pulse forms and the typical forward breakdown pattern are also shown in this figure. The timing of the triggering circuit was adjusted so that the tube V2 had a forward voltage on it for a relatively long time (up to 15 msec at 60 pps). For V1, four 5552 tubes were used in parallel to prevent any breakdown. It was found that the 4681 tube broke down first in the reverse direction when negative voltage was applied to its anode as either the temperature or the repetition rate was increased.

It is interesting to note that the breakdown occurred with the largest probability at time $t = 0$, when the high voltage positive pulse

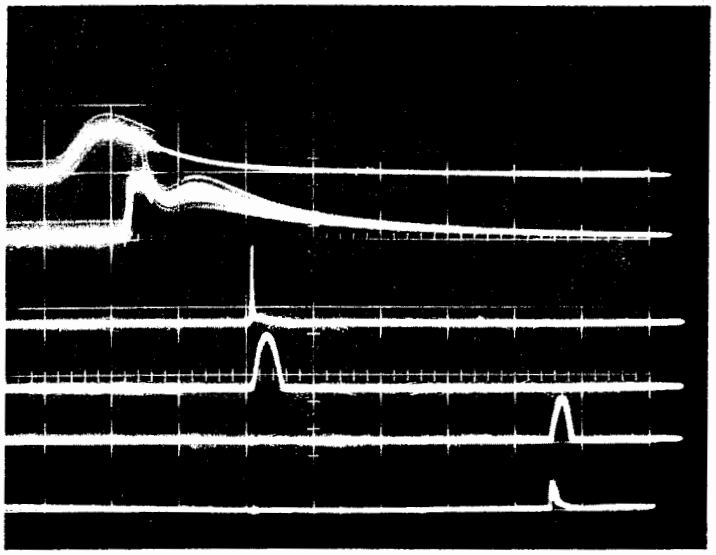

Fig. 12a--T = 8°C, repetition rate = 360 pps. Sensitivities are the same as in Fig. 10b.

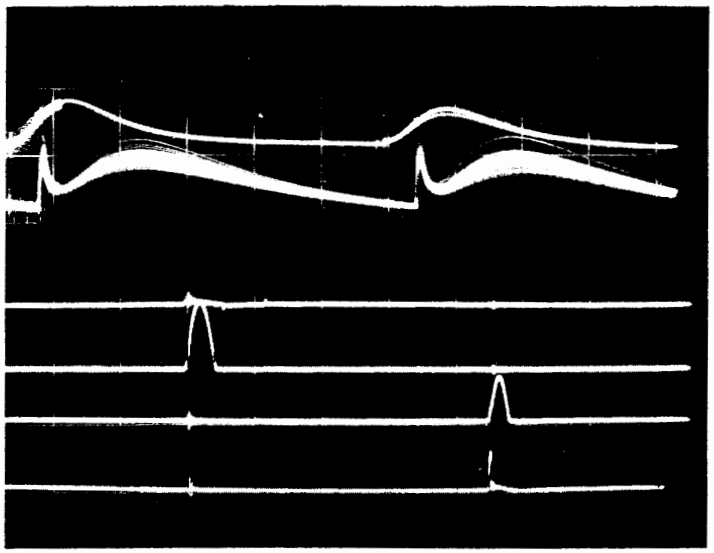

Fig. 12b--T = 25°C, repetition rate = 360 pps. Sensitivities are the same as in Fig. 10b.

Fig. 12--Anode current wave forms.

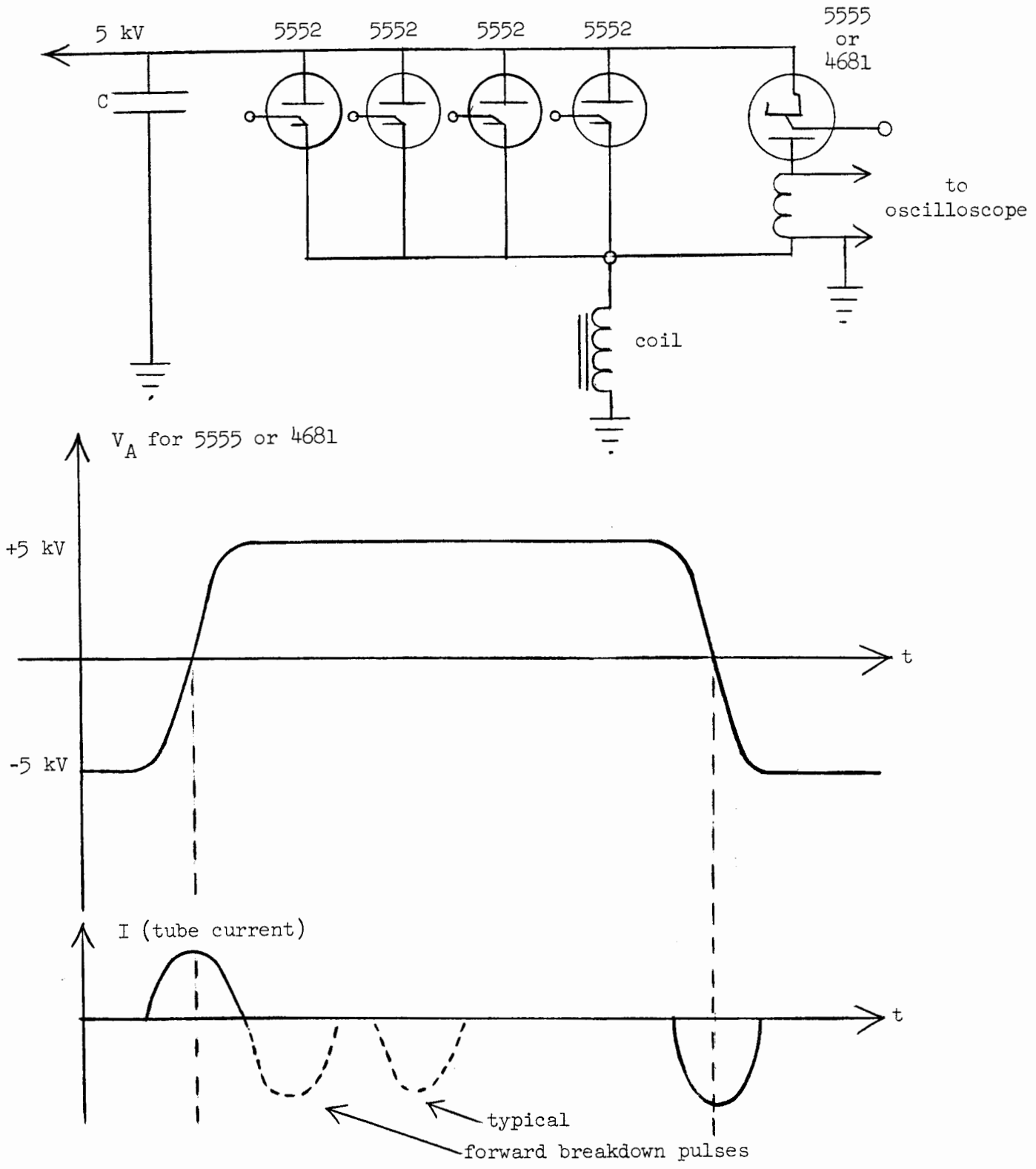

Fig. 13--Test circuit for forward-breakdown study.

was applied on the anode, and it decreased with time as shown in Fig. 14. Breakdowns were observed even 10 ms after the application of the voltage to the tube. However, with increasing temperature, peak current (I_o), or repetition rate, the frequency of the breakdown sharply increased at $t = 0$ and later decreased to zero. Beyond an initial value of T, I_o, and repetition rate, the tube failed immediately after the application of high voltage. Typical time distribution of this forward breakdown is shown in Figs. 15a and 15b.

In order to explain this breakdown mechanism, one can assume a storage mechanism as the cause of the breakdown. This mechanism can be initiated by high repetition rate, peak current, or pressure in the tube for several milliseconds after the conduction period (up to 16 msec). It is hard to imagine that any charged particle storage time in the tube could be so long.

From Paschen's theory, one would expect that the breakdown voltage at $T = 38^{\circ}C$, $p = 4.4 \times 10^{-3}$ mm Hg, $pd \approx 10^{-2}$ would be of the order of 30 to 70 kV, which is very close to the static limit and in any case is much larger than the few kV (2 to 5 kV) that were observed. In the following table the breakdown voltage is estimated for the 5555 tube as a function of pd, with $d \approx 10$ cm.

TABLE I

BREAKDOWN VOLTAGE, 5555 TUBE

T(°C)	p	pd	V_B	Note
20	1.1×10^{-3}	1.1×10^{-2}	> 50 kV	From Paschen's Theory (Thermal Equilibrium Condition)
40	5.0×10^{-3}	5.0×10^{-2}	≈ 50 kV	
60	2.5×10^{-2}	2.5×10^{-1}	≈ 10 kV	
80	9.0×10^{-2}	9.0×10^{-1}	≈ 3 kV	
100	2.77×10^{-1}	2.77×10^{-1}	≈ 1 kV	

It is evident from this table that the tube would not break down unless the pressure in the tube increased even temporarily during the operation to close to 9×10^{-2} mm Hg, and this higher pressure should last only a

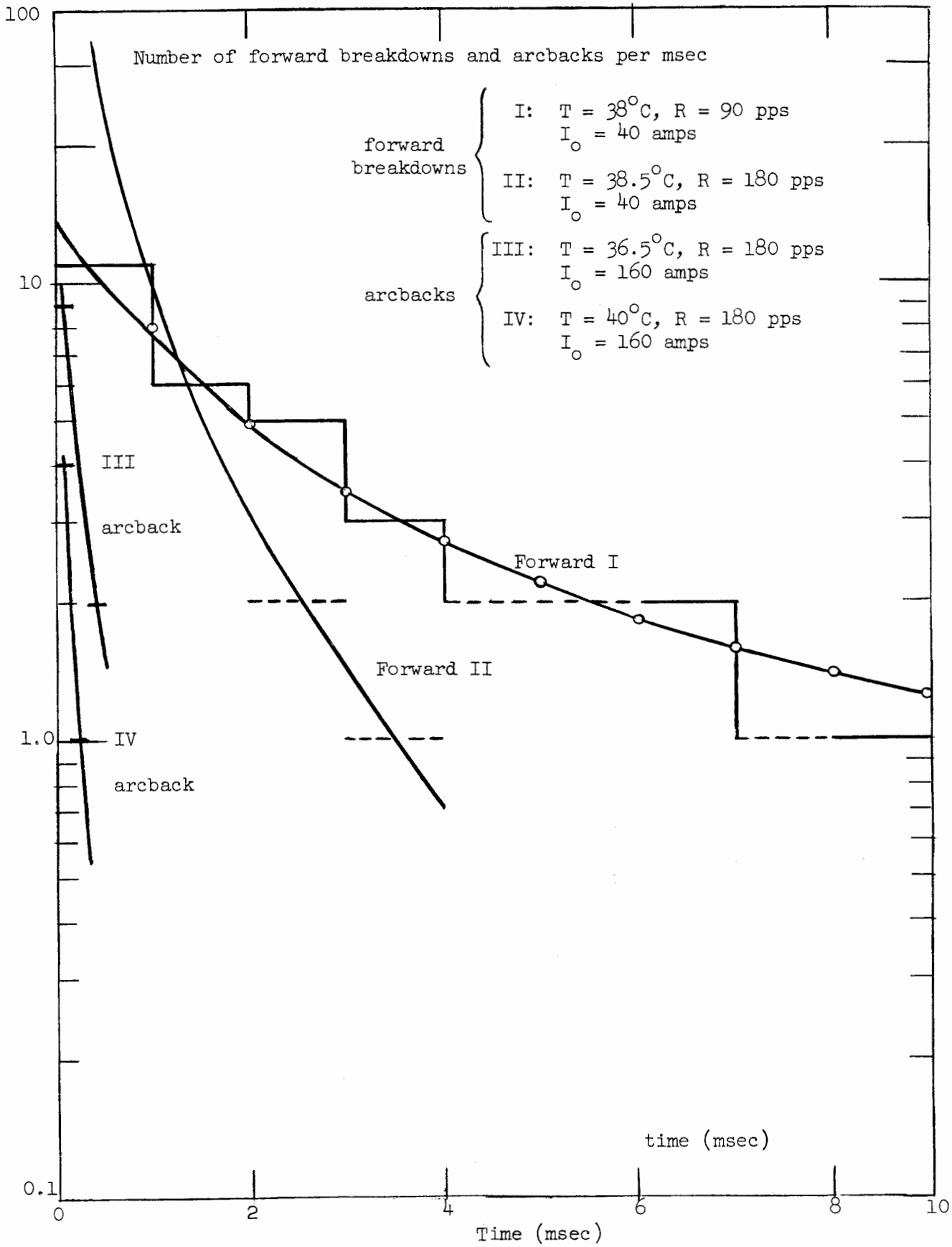

FIG. 14--Breakdown rate.

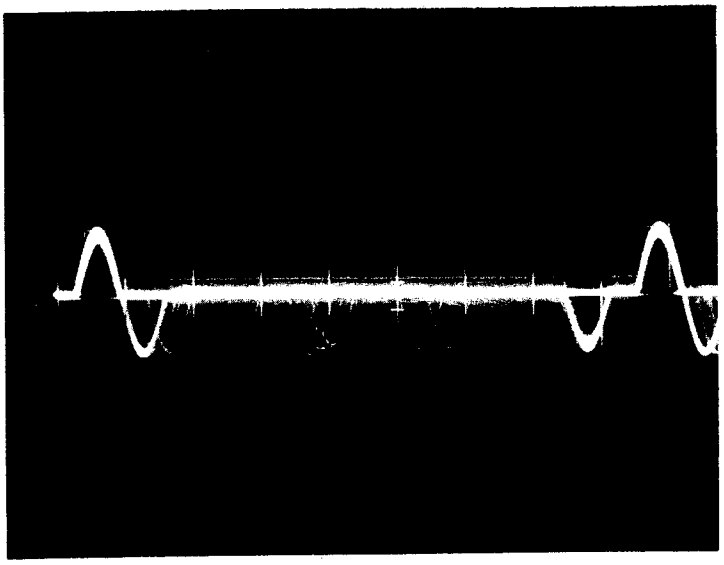

Fig. 15a--Time distribution of the forward breakdowns. T = 38°C, repetition rate = 90 pps, sensitivity = 50 amps/cm, 1 msec/cm. The exposure time is 5 sec. Tube 5555.

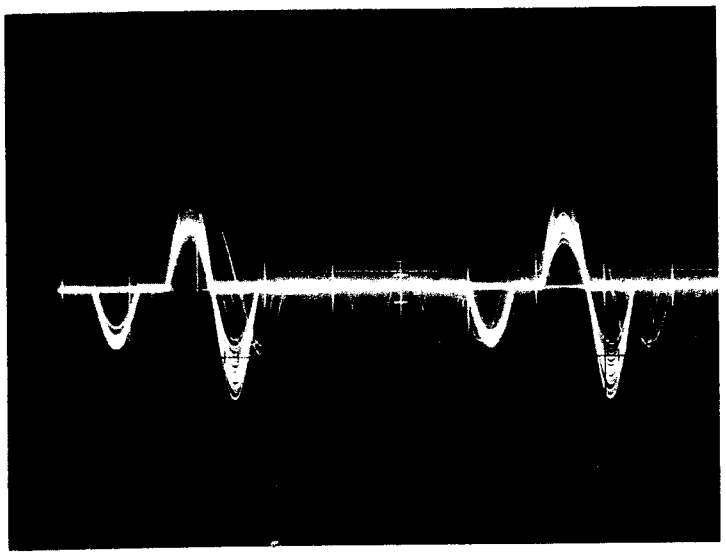

Fig. 15b--Time distribution of the forward breakdowns. T = 38.5°C, repetition rate = 180 pps, sensitivity = 50 amps/cm, 1 msec/cm. The exposure time is 5 sec. Tube 5555.

Fig. 15--Time distribution of forward breakdowns.

few milliseconds.

It is well known[10] that during the conduction cycle the mercury from the cathode pool is vaporized at a rate of approximately 7×10^{-3} grams per coulomb, and that this mercury blast creates a pressure far in excess of the pressure as determined by the temperature. The mechanism of the pressure increase during and after the conduction may be explained as a result of the thermalization of the fast vapor stream due to the energy losses suffered in scattering processes. The baffle in the tube helps to randomize the unidirectional flow, and the thermalization process is even more effective; the transient pressure build-up can therefore be longer. This mechanism gives a natural explanation of the observations that the tube with a baffle breaks down more easily in the forward direction than the tube which does not contain any obstacle between the cathode and anode region. Under operating conditions it is possible for a pressure build-up to occur which will actually increase pd and with this cause a decrease in the maximum voltage value that the tube can hold off without breaking down. However, it is necessary to explain the fact that this transient pressure rise has a time constant of sufficient length to cause breakdowns 1 to 10 msec later. In order to calculate the time constant for the transient pressure rise, it is assumed that the main loss mechanism for neutral particles from the cathode-anode region is the diffusion to the walls. Let the particle density after the conduction cycle commences be $n(r,x,t)$ in the cathode-anode region. Then for a cylindrical volume with radius r_o and length ℓ (cathode-anode distance), the solution for the lowest diffusion mode can be written as

$$n = n_o \cos axJ_o(br)e^{-\frac{t}{\tau}}$$

where $a^2 + b^2 = (1/D\tau)$ and τ is the decay constant. Inserting boundary condition, $n = 0$ at the walls of the cylinder of radius r_o and height ℓ, then

$$a = \left(\frac{\pi}{\ell}\right), \quad b = \left(\frac{2.405}{r_o}\right)$$

and

$$\left(\frac{1}{D\tau}\right) = \left\{\left(\frac{\pi}{\ell}\right)^2 + \left(\frac{2.405}{r_o}\right)^2\right\} = \frac{1}{\Lambda^2} = \frac{1}{\Lambda_\ell^2} + \frac{1}{\Lambda_{r_o}^2}$$

For the decay constant one obtains,

$$\tau = \frac{1}{D}\left\{\left(\frac{\pi}{\ell}\right)^2 + \left(\frac{2.405}{r_o}\right)^2\right\}^{-1} = \frac{\Lambda^2}{D}$$

noting that the diffusion coefficient of neutral gases changes with the pressure and temperature as[1]

$$D(p_1 T) \approx D_o \left(\frac{T}{T_o}\right)^m \left(\frac{p_o}{p}\right)$$

where D_o is the value of D at $T = 273^\circ K$, $p_o = 760$ mm Hg, and $m \approx 1.5 - 1.75$. The decay constant can now be written as a function of the pressure in the following form:

$$\tau = \frac{1}{D_o\left(\frac{T}{T_o}\right)^m p_o} \frac{p}{\left\{\left(\frac{\pi}{\ell}\right)^2 + \left(\frac{2.405}{r_o}\right)^2\right\}}$$

For example, the self-diffusion coefficient of Hg in Hg can be calculated from the value of D for mercury gas diffusion in air,[11] for which

$$D_{\text{Hg in Air}} = 0.1124 \text{ cm}^2/\text{sec} = 0.59\sqrt{\frac{M + m}{mM}}$$

where m is the diffusing agent and M is the mass of the gas atoms. Then for Hg self-diffusion, one obtains

$$D_{\text{Hg in Hg}} = 0.59\sqrt{\frac{200 + 200}{4 \times 10^4}} = 0.059 \text{ cm}^2/\text{sec}$$

With $\ell \approx 10$ cm and $r_o \approx 5$ cm, one obtains at $T = 38^\circ C$ and $T = 80^\circ C$,

$$\tau_{38^\circ} \approx \frac{p(mm)}{14.7} = 3 \times 10^{-4} \text{ sec} = 0.3 \text{ msec}$$

$$\tau_{80^\circ} \approx \frac{p(mm)}{14.7} = 6.8 \times 10^{-3} \text{ sec} = 6.8 \text{ msec}$$

The large value of τ clearly shows that at the elevated non-equilibrium pressure condition, a pressure build-up is possible when the repetition rate is higher than $1/\tau$, because the main loss mechanism is not sufficient to reduce the pressure between pulses. The mechanism of the thermalization of the fast vapor stream still remains to be answered.

As mentioned before, the slowing down of the vapor atoms is the consequence of the energy loss in atom-atom collisions. The average number of collisions required to slow down an atom from an energy E_o to thermal energy $E_1 = 0.025$ eV is given by the following formula

$$C = \frac{\ell n(E_o/E_1)}{\xi}$$

where

$$\xi = 1 + \frac{\frac{E_1}{E_o} \ell n \frac{E_1}{E_o}}{1 - \frac{E_1}{E_o}} \approx 1$$

is the average logarithmic energy change per collision. With $E_o = 0.5$ to 50 eV, the C changes from 3 to 7.6. One can then safely say that less than 10 collisions are sufficient for thermalization. The mean free path of atoms ($p = 4.4 \times 10^{-3}$ mm Hg) is $L_{38^\circ} = 6.45 \times 10^{-1}$ cm at $T = 38^\circ C$ and $L_{80^\circ} = 2.82 \times 10^{-2}$ cm at $T = 80^\circ C$, then the thermalization distance is

$$L_{Th} < 6.45 \text{ cm at } T = 38^\circ C$$

and

$$L_{Th} < 2.82 \times 10^{-1} \text{ cm at } T = 80^{\circ}C \ .$$

The increasing effectiveness of the thermalization and the diffusion time-constant with increasing temperature can explain the fact that there is a definite limit in repetition rates even when the duty cycle remains constant, i.e., the pulse length decreases with increasing pulsing rate. This can be seen from the following: It was mentioned before that approximately 7 mg of mercury leave the cathode pool per one coulomb of charge arriving at the cathode. Then the number of the atoms leaving the point-like cathode spot ($r \approx 10^{-3}$ cm) in one conduction cycle is

$$N' = \frac{7 \times 10^{-3} I_o T_p}{M_{Hg}}$$

where I_o is the pulse current, T_p is pulse length and M_{Hg} is the mass of the Hg atom. If $P(L_{Th})$ is the probability of the thermalization, the number of the atoms contributing to the transient density is $P(L_{Th})N'$, and the transient density is given by

$$n' = P(L_{Th}) \frac{N'}{V}$$

where V is the tube volume. In order to obtain a functional relationship between the operating parameters, let us suppose that n' is small compared to the equilibrium density n. Then the transient density is given after N pulses ($N = Rt$), or at time t_1 as

$$\int_0^{t_1} Nn'e^{-\frac{t}{\tau}} = Nn'\tau\left(1 - e^{-\frac{N}{R\tau}}\right)$$

This, however, must be smaller than a given value to prevent breakdown.

One can therefore write

$$f\left\{Nn'\tau\left[1 - e^{-\frac{N^-}{R\tau}}\right] I_o T_{pp}(T)\right\} \leq \text{constant} .$$

From this it is evident, even in this crude approximation, that the forward breakdown is a very sensitive function of the repetition rate R and the temperature T.

V. PLASMA FORMATION AND DEIONIZATION

The conduction cycle in the ignitron begins with the firing of the ignitor to form a cathode spot and generate electrons in order to start an avalanche to the anode. Electrons arriving near the anode come under the influence of the anode field where an increased ionization and avalanche formation take place. The increased ionization and avalanche formation finally develop into a low pressure arc discharge. The discharge lasts until the pulse forming network delivers energy through the load. The fact that a much smaller field than that necessary for breakdown is usually required to maintain the plasma suggests that the ionization efficiency is larger. One possible mechanism that reduces the escape rate of the electrons in the conduction cycle is a change from the free electron diffusion to an ambipolar diffusion. In this case the drift velocity of the plasma constituents is neither that of the ion, nor that of the electron but is determined by the ambipolar diffusion coefficient. The effective diffusion coefficient common to both electrons and ions can be written as

$$D_A = \frac{\mu^+ D^- - \mu^- D^+}{\mu^+ - \mu^-}$$

or, using the fact that the mobilities of the ion μ^+ and electron μ^- are related to the corresponding diffusion coefficients D^+ and D^-, one can write

$$D_A = \frac{D^+ D^- \left[(1/kT_+) + (1/kT_-)\right]}{(D^+/kT_+) + (D^-/kT_-)} \approx D^+\left(\frac{T_-}{T_+}\right)$$

where $T_- > T_+$ and

$$\frac{D^+}{kT_+} = \frac{\mu_+}{e} < \frac{\mu_-}{e} = \frac{D^-}{kT_-}$$

In order to get a value for D_A, one must estimate the electron temperature in the plasma, where the ambipolar diffusion is the dominant loss mechanism. One might start with the diffusion equation

$$-D_A \Delta^2 = \nu_i u$$

or

$$\frac{D_A}{\Lambda^2} = \nu_i$$

with

$$\frac{1}{\Lambda^2} = \left\{ \left(\frac{\pi}{\ell}\right)^2 + \left(\frac{2.405}{r_o}\right)^2 \right\}$$

$$= \left(\frac{2.405}{R_o}\right)^2_{eff}$$

where R_o is an effective radius for the plasma vessel and ν_i is the ionization frequency. ν_i is defined by the relation

$$\nu_i = p \int_o^\infty P_i(v) F(v) V dv$$

where $P_i(v)$ is the probability of the ionization, and $F(v)$ is the energy distribution function. Using a Maxwellian energy distribution for the fast electrons, a relation can be derived[12] between U_I/T_e and the product of $C \cdot p \cdot R_o$, where C depends on the particular gas used.

For mercury the first ionization potential is $U_I = 10.4$ volts. The equation is

$$\frac{1}{\sqrt{\frac{e \cdot U_I}{kT_e}}} e^{\frac{eU_r}{kT_e}} = 1.16 \times 10^7 C^2 \cdot p^2 \cdot R^2$$

with $C = 11 \times 10^{-2}$; this formula is plotted in Fig. 16 in the form of $T_e/U_I = f(C \cdot p \cdot R)$. Using the pressure values of 4.4×10^{-3} mm and 0.1 mm, and $(R_o)_{eff} = 5$ cm, the electron temperatures calculated from Fig. 16 are given as

$$T_e \approx 23{,}000^\circ K \quad \text{at} \quad p = 4.4 \times 10^{-3} \text{ mm Hg}$$

$$T_e \approx 10{,}000^\circ K \quad \text{at} \quad p = 0.1 \text{ mm Hg}$$

One should realize that these values are approximate and are true only in a pressure region where there are enough collisions to establish the diffusion and $\nu_i \propto p$. This means that no ionization is produced by light emitted by excited states, because in that case $\nu_i \propto p^2$.

Using these electron temperature values, the ambipolar diffusion coefficient can be estimated as

$$D_A = D_+ \left(\frac{p_o}{p}\right) \left(\frac{T_-}{T_+}\right) \approx \frac{D}{5} \left(\frac{p_o}{p}\right) \left(\frac{T_-}{T_+}\right)$$

$$D_A = 1 \times 10^{-2} \left(\frac{760}{p}\right) \left(\frac{T_-}{1500}\right)$$

where it is assumed that the ion temperature is of the order of $1500^\circ K$. With these values, where the electron temperature $T_- = 23{,}000^\circ K$, the diffusion time-constant will be

$$\tau_{Diff} = \frac{5\Lambda^2}{D\left(\frac{T_-}{T_+}\right)} = \frac{\Lambda^2}{D_A}$$

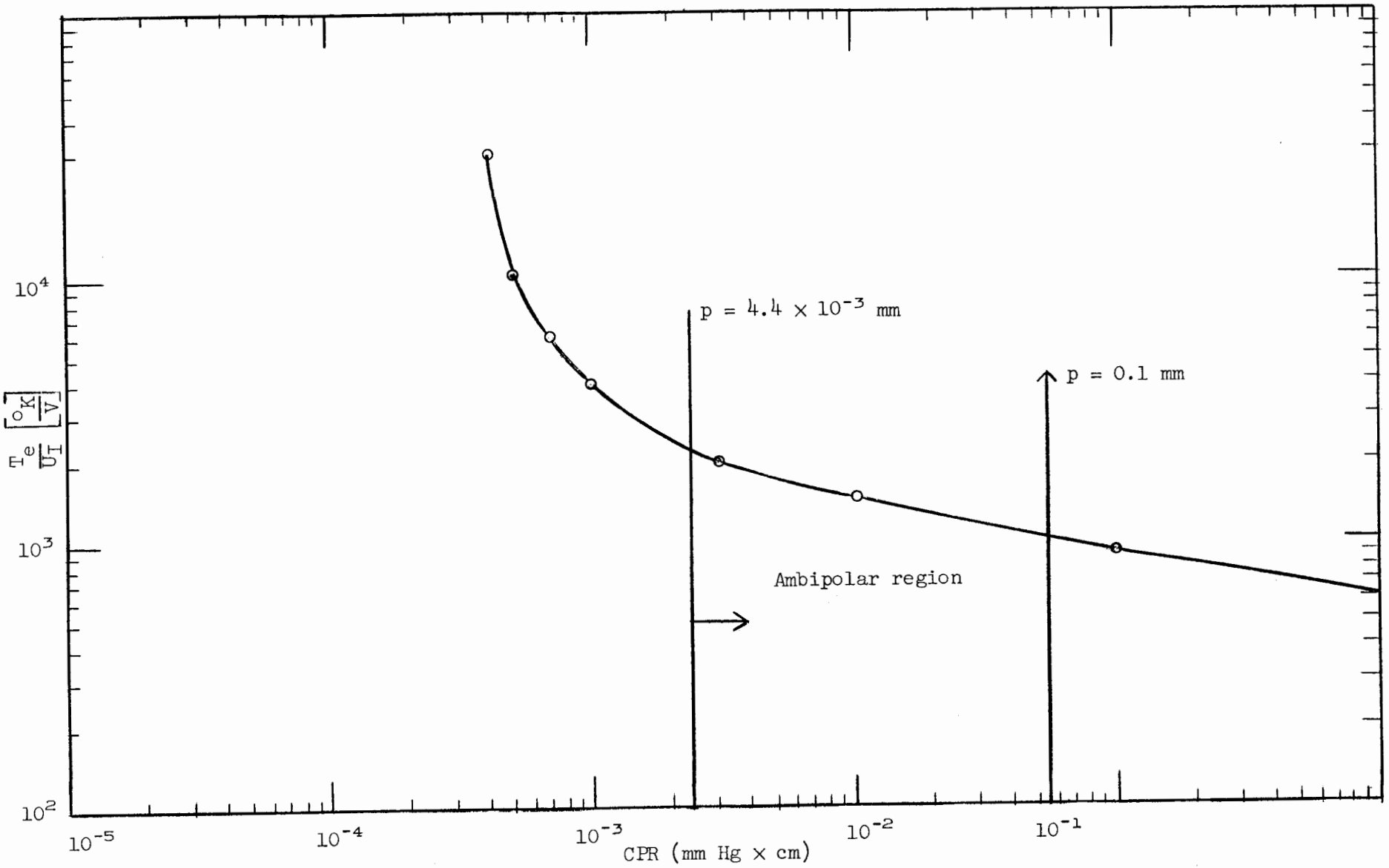

Fig. 16--Ratio of electron temperature to ionization potential vs mercury vapor pressure.

and from this

$$\tau_{Diff} \approx \quad 30 \ \mu sec \text{ at } 20^{\circ}C$$

$$\tau_{Diff} \approx \quad 115 \ \mu sec \text{ at } 38^{\circ}C$$

$$2_{Diff} \approx 4000 \ \mu sec \text{ at } 80^{\circ}C$$

This time-constant cannot be identified with the deionization time because other processes, such as the recombination and convection current to surfaces, can reduce the ion or electron density after the conduction cycle. The deionization time-constant is actually composed of the decay constants of these processes in the form

$$\frac{1}{\tau_D} = \frac{1}{\tau_{Diff}} + \frac{1}{\tau_{conv}} + \frac{1}{\tau_R}$$

In order to estimate the deionization time, one must obtain information about the ion and electron density, Debye length, and other parameters for the plasma.

The ion density as a function of the temperature is plotted in Fig. 8, after Langmuir[13] and Killian,[14] where the electron and ion density are taken to be equal in order to insure the neutrality of the system. These quantities can be calculated from the measured current density using the formula

$$J_- = 2.46 \times 10^{-14} n_- \sqrt{T_e} \qquad \text{amps/cm}^2$$

or from the voltage drop across the tube, using some simple model for the microfield distribution in the plasma.

The recombination of positive ions with thermal electrons is governed by the following relation[15]

$$\frac{dn(t)}{dt} = \alpha n_+^2 \qquad \text{sec}^{-1} \ \text{cm}^{-3}$$

where

$$\alpha = 5 \times 10^{-22} \frac{1}{\left(\frac{T_e[^oK]}{1000}\right)} \qquad cm^3/sec$$

After integration, the ion density as a function of time is given by

$$n(t) = \frac{n}{1 + \alpha n t} = \frac{n}{1 + t/\tau_R}$$

where n is the concentration of ions at the instant the source of ionization is removed, and τ_R is the recombination time-constant.

At $T = 80^oC$; $n = 1.5 \times 10^{13}(cm^{-3})$

$$\tau_R = \frac{1}{n\alpha} \approx 4.4 \times 10^{12} \text{ sec}$$

thus $\frac{1}{\tau_R}$ is negligibly small. The physical reason for the small amount of deionization due to volume recombination is the high energy of the plasma electrons. The deionization time, neglecting the effect of the volume recombination, can then be computed from

$$\frac{1}{\tau} = \frac{1}{\tau_{Diff}} + \frac{1}{\tau_{conv}}$$

In order to calculate τ_{conv}, one assumes that electrodes (probes) can become negative relative to the plasma after the conduction cycle. This is the case with tube V2, where its anode becomes negative and acts as a negative probe.

The positive ion current density to the negative "anode" (back-current density) has two components: One is the directed convection current density

$$j_1^+ = \frac{en^+\bar{v}^+}{4}$$

where $\bar{v}^+$ is the average ion velocity at the plasma sheath; the other component is displacement current density which is due to the time dependence of the Debye length, namely

$$j_2^+ = en^+ \frac{dh}{dt} \quad \text{where} \quad h^2 = \frac{kT_e}{4\pi n^+ e^2}$$

Adding the displacement current, which is due to the change in charge density on the anode, the following expression for the positive ion current density, which now includes all the components, is obtained.

$$j^+ = e \frac{D_A}{\Lambda} n^+ \frac{en^+\bar{v}_+}{4} + en^+ \frac{dh}{dt} + \epsilon_o \frac{dE}{dt}$$

This equation can be integrated from the time at which the plate voltage is nearly constant (10 to 30 μsec after the conduction begins) because then $dE/dt = 0$, and assuming that the Debye length increases linearly in time or dh/dt is constant. Using current conservation one can write

$$e \frac{\partial n_+}{\partial t} = -\text{div } j^+ = -e \left[\frac{D_A}{\Lambda^2} + \frac{\bar{v}_+}{4\Lambda_\ell} + \frac{1}{\Lambda_\ell} \frac{dh}{dt} \right] n_+$$

which after formal integration gives

$$n_+(t) = n_o^+ e^{-\frac{t}{\tau_D}}$$

where n_o^+ depends on primary ionization (or peak current I_o through the tube), and

$$\tau_D^{-1} = \frac{D_A}{\Lambda^2} + \frac{\bar{v}_+}{4\Lambda_\ell} + \frac{1}{\Lambda_\ell} \frac{dh}{dt} = \frac{1}{\tau_{Diff}} + \frac{1}{\tau_{conv}}$$

The first term is the inverse of the familiar diffusion time-constant, the second and third terms are the inverse of the convection time-constant that originated from the fact that space charge limited current-flow can decrease the ion density near a charged electrode in the plasma.

To get order-of-magnitude values for τ_{conv} one can estimate the following quantities:

$$\frac{4\Lambda_\ell}{\bar{v}_+} = \frac{4 \times 10^{-1}}{1 \times 10^{5}} \approx 4 \times 10^{-6} \text{ sec}$$

where[16]

$$\bar{v}_+ = \alpha \left(\frac{kT_e}{n_+}\right)^{\frac{1}{2}} \quad \text{and} \quad \alpha \sim 1.0$$

and

$$\left(\frac{1}{\Lambda_\ell}\frac{\partial h}{\partial t}\right)^{-1} \approx \frac{\Lambda_\ell \Delta t}{\Delta h} \approx 10^{-5}$$

where it is assumed that the Debye thickness changes linearly in time from 10^{-3} cm to 1 cm during the deionization time (~100 μsec). With these assumptions

$$\tau_{conv} = \frac{4 \times 10}{4 + 10} \approx 28.6 \text{ μsec}$$

Using these numbers, the current density flowing to the negative "anode" can be written as

$$j^+ = j_o^+(I_o) e^{-\frac{t}{\tau_{Diff}} - \frac{t}{\tau_{conv}}} + \epsilon^o \frac{dE}{dt}$$

where ϵ^o is the permittivity of the free space. The peak current density j_o^+ depends on the rate of ionization, pressure, and peak current during the conduction cycle.

VI. MECHANISM OF THE BACKFIRE (ARCBACK)

It was mentioned earlier that at high repetition rate (360 pps) and high peak current operation the ignitron breaks down in the reverse direction when reverse voltage is applied to tube V2 after the normal conduction cycle. The frequency of the arcbacks increases sharply with peak current and repetition rate at constant anode voltage. The circuit used to measure the frequency of the backfires and the ion current to the negative "anode" is shown in Fig. 17. The frequency-time distribution of the arcbacks is markedly different from the forward breakdown frequency-time distribution (see Fig. 14). The arcbacks occurred with a very high probability just after application of the reverse voltage (after the forward conduction cycle) and the probability of breakdown is very small after 100 to 300 microseconds. Typical pictures of the current traces are shown in Fig. 18. The backfires were usually followed by forward breakdowns as shown in Figs. 18a and 18b.

The arcback can be defined as a failure of the voltage-holding capability of the tube in the reverse direction. This results in a flow of an electron current in the reverse (anode to cathode) direction, due to the formation of a cathode spot on the anode.

It is believed by the authors that the primary cause of the arcback is the positive ion current flowing to the anode after the normal conduction cycle ends and the negative potential (reverse voltage) starts to build up on the anode. Possible mechanisms for the cathode spot formation on the anode were investigated by others and the dominant processes can be listed as follows:

1. Kingdon and Lawton in their classical paper[17] proposed that the arcbacks are due to the collection of positive ions on small insulating patches on the anode. If the potential gradient exceeds the field emission limit of the anode material, electron emission can start from this "cathode spot" and this emission can result in arcback. The probability of spot formation naturally depends on the ion density after the conduction on the anode voltage, and on charge leakage from the insulating particles. Kingdon and Lawton state that the rate of arcback is proportional to the product of the initial inverse voltage (anode

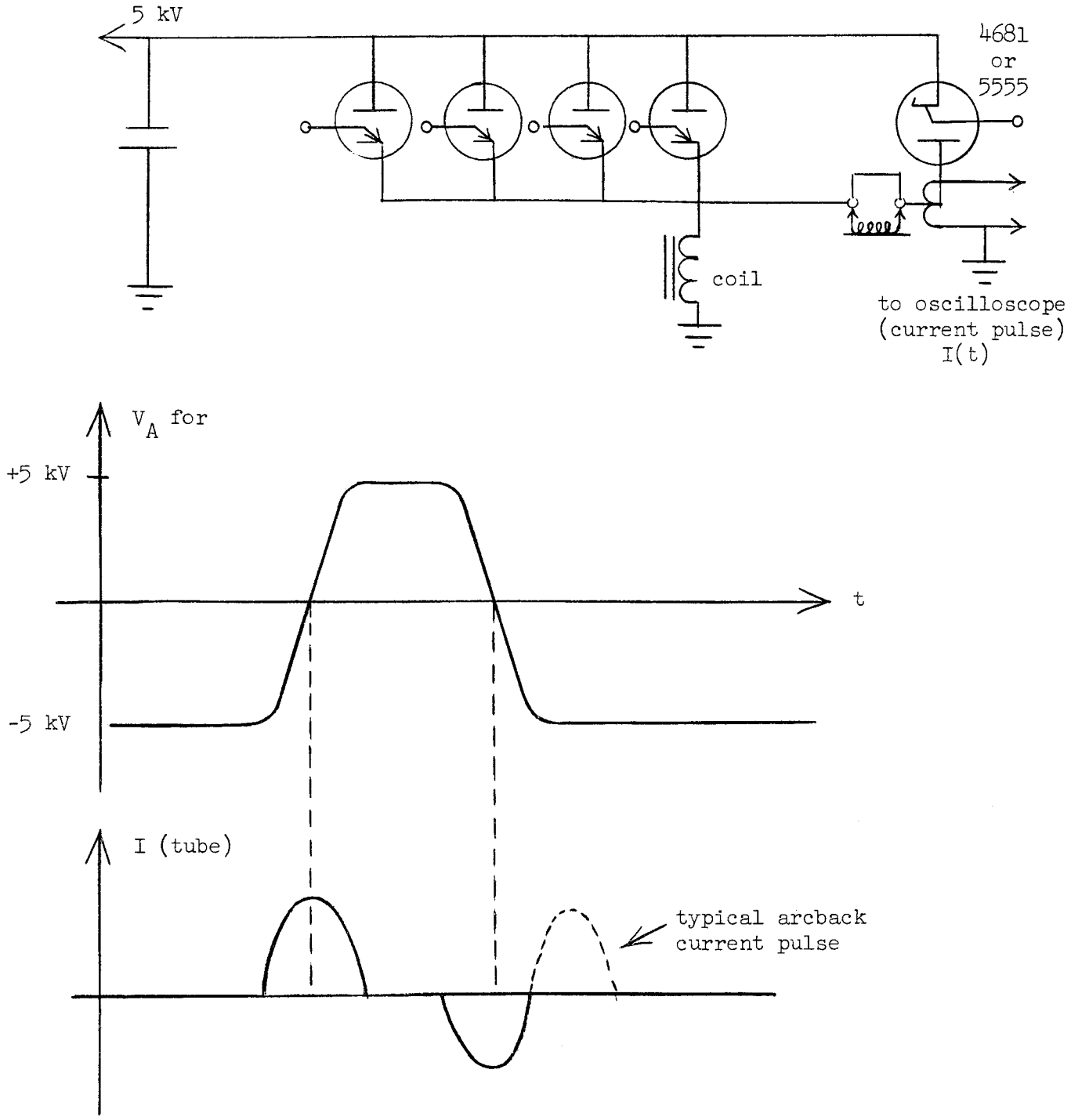

Fig. 17--Test circuit for arcback study.

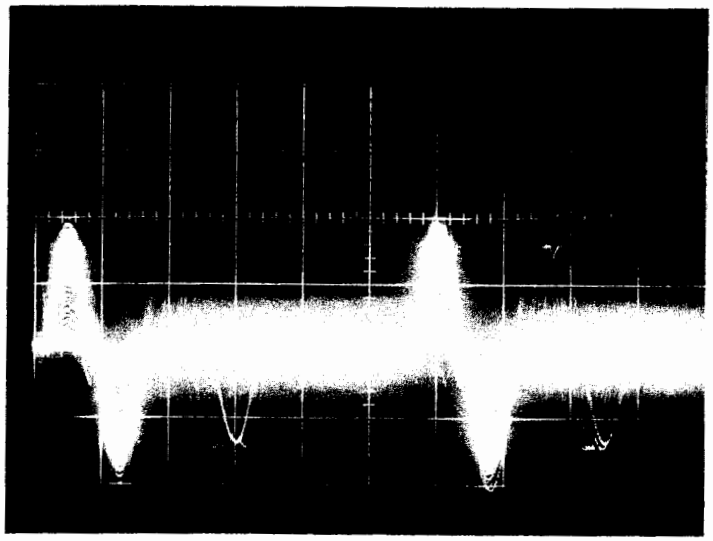

Fig. 18a--Typical current trace of 4681 ignitron in case of reverse breakdown. This picture is a 90 sec time exposure. Sensitivity 100 amps/cm, 1 msec/cm. Repetition rate 180 pps. The cooling water temperature is $T = 36.5^{\circ}C$.

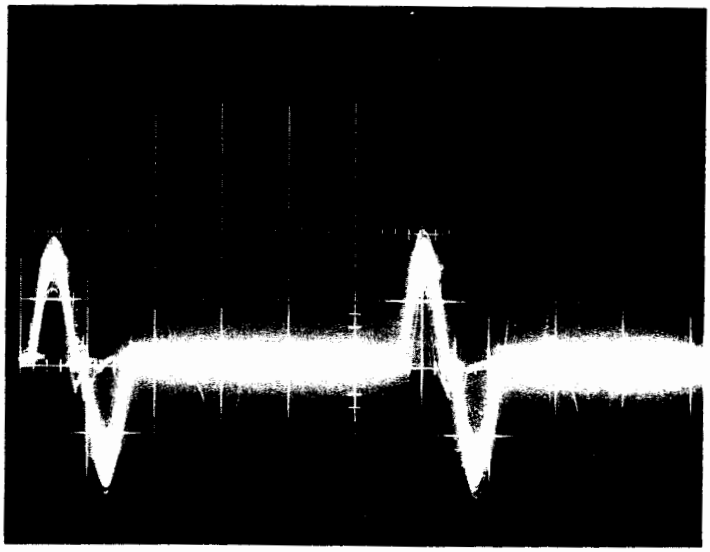

Fig. 18b--Current trace of the 4681 ignitron in the case of reverse breakdown. Exposure time is 30 sec. Sensitivity 100 amps/cm, 1 msec/cm. The repetition rate is 180 pps and the water temperature $T = 40^{\circ}C$.

Fig. 18--Typical current traces of the 4681 ignitron in case of reverse breakdown.

voltage) and the rate of the current (forward) charge. This can be expressed in terms of an arcback factor δ as

$$\delta = V \frac{dI}{dt}$$

where

V = negative anode potential at the end of the forward conduction cycle in kilovolts

$\frac{dI}{dt}$ = rate of current charge at the end of the forward conduction cycle in amperes per microsecond

This theory is proved by many experiments[18] in ignitron rectifier service operation, but needs some extension to explain the significance of the Kingdon factor δ in modulator service.

2. It was observed[19] that mercury droplets on the anode surface can initiate arcbacks. These droplets collect ions and can cause large gradients when leaving the anode. To prevent the accumulation of these mercury droplets on the anode surface, a baffle is used in the tubes.

3. Thermal emission from the anode due to local heating.

In addition to these processes, there are several secondary effects connected with impurity conditions in the tube which can aid in the development of cathode spots on the anode.

In extension to these mechanisms for cathode spot formation, we would like to propose another process in which the spot formation starts with electron collection on small insulating patches on the anode. The electrons are collected on these insulating surfaces during the normal conduction cycle and stored until the potential of the anode reaches 0. This is possible because the time constant of electron surface charge density on dielectric surfaces can be as large as 100 to 1000 μsec,[20] but the time required for the potential change on the anode from a small positive voltage (voltage drop during the conduction ~10 to 100 volts to -5 kV is only 10 to 30 μsec. Now if the potential on this insulating surface is V, the electron current density to the particle is

$$j_- = \frac{n_- e \bar{v}_-}{4} e^{-\frac{eV}{kT}}$$

where

$$v_- = \left(\frac{8kTe}{\pi m_-}\right)^{\frac{1}{2}}$$

and the ion current density is given by

$$j_+ = n_+ e\bar{v}_+ = \alpha \left(\frac{kTe}{m_+}\right) n_+ e \quad \text{where} \quad \alpha \approx 1$$

When the net current to the surface of the particle is zero, the negative potential does not increase further and the potential between the particle and the surface is given by the floating potential[21] V_f, which is

$$V_f = \frac{kTe}{2e} \ell n \left(\frac{m_+}{2\pi m_-}\right) \approx 8 \text{ volts} \quad \text{when} \quad Te \approx 16{,}000^\circ K$$

and the field between the plasma and the particle surface is

$$E \approx \frac{V_f}{\text{Debye length}} \approx \frac{10}{10^3} = 10^4 \text{ volts/cm}$$

This large field strength can further increase the ion current to the particle and might initiate local electron emission from the surface. If the floating potential V_f exceeds the potential difference required to sustain an arc, a unipolar arc formation[22] might start. Either the electrons emitted from the surface or the electrons from the arc can start an avalanche to the positive cathode and the tube breaks down in the reverse direction. Because this process involves electron deposition on the anode impurities, it must start before the application of the negative potential on the anode; however, the actual breakdown occurs when the potential on the anode is 0 or negative and the positive ion current is flowing to an impurity surface. If this type of cathode spot formation is possible, one would expect all the arcbacks within the electron storage time (100 to 1000 μsec) to occur on the insulating surface.

From these possible cathode spot formation mechanisms it can be seen that the positive ion current flowing to the negative anode plays an important role. This ion current was measured using the circuit shown in Fig. 17. Typical pictures of the ion-current and the plate voltage

wave-forms are shown in Figs. 19a and 19b. Part of the forward current wave-form during the conduction cycle is also shown on the top traces. The damped oscillation wave-form which can be seen on both traces is due to the ringing of the coil inductance with its stray-capacitance. Figures 20a and 20b show the trace of the ion-current (top traces) when a saturable reactor L is in series with the anode. The space charge limited flow is clearly observable on these photographs. The saturable reactor in the circuit slows down the anode voltage rise-time to 20 μsec as compared to the rise-time of about 10 μsec when no reactor is in the circuit, and increases the decay-time of the forward current pulse. The longer rise-time results in a decrease in the peak ion current from 2.5 to 0.6 amps, using the same value of peak forward current $I_o = 160$ amps. From these pictures it is evident that the decay of the positive ion current is the superposition of two decay processes with time constants of $\tau_1 \approx 20$ to 30 μsec and $\tau_2 \approx 70$ to 100 μsec. The decay of the ion current at different forward peak current values without the saturable reactor is shown in Fig. 21, and with the saturable reactor in Fig. 22. These measured decay constants ($\tau_1 \approx 30$ μsec, $\tau_2 \approx 70$ to 100 μsec) can be identified as the time constant of the space charge limited ion flow, and the ion diffusion time constant. The calculated values for the time constants are

$$\tau_{conv} \approx 28.6 \text{ μsec}$$

$$\tau_{Diff} \approx 30 \text{ to } 115 \text{ μsec}$$

which are very close to the measured values. Figure 23 shows the dependence of the peak ion current on the peak forward current at different temperatures, with or without the saturable reactor. In the next chapter the dependence of the peak current on the circuit elements will be discussed in connection with the Kingdon factor. In summarizing the results of this section, it may be said that in order to prevent the arc-backs, which are primarily caused by the back-streaming ion current to the negative anode, one should eliminate or at least minimize this ion current. The time-dependence of this ion current is governed by the

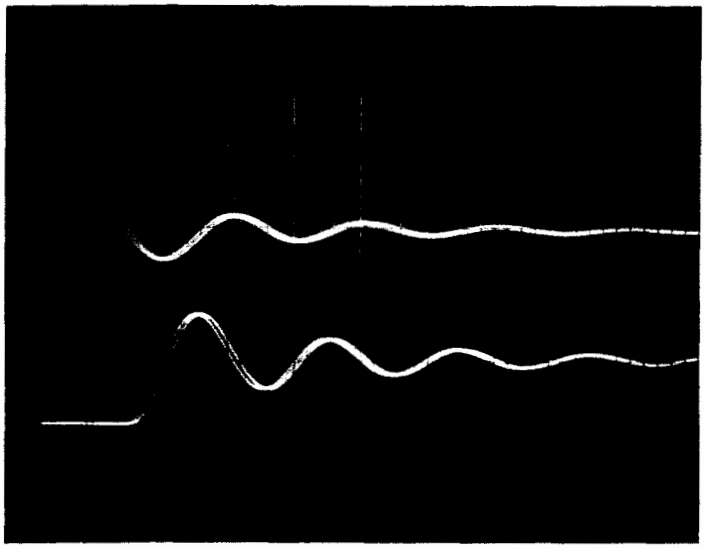

Fig. 19a--On the top trace the time dependence of the positive ion current is shown for the 5555 tube. Part of the forward current wave form can be seen also. The forward peak current is I_o = 160 amps and the sensitivity is 5 amps/cm, 10 μsec/cm. The bottom trace shows the plate voltage wave form. The sensitivity is 5 kV/cm and the sweep is 10 μsec/cm. T = 20.8°C and the repetition rate is R = 90 pps.

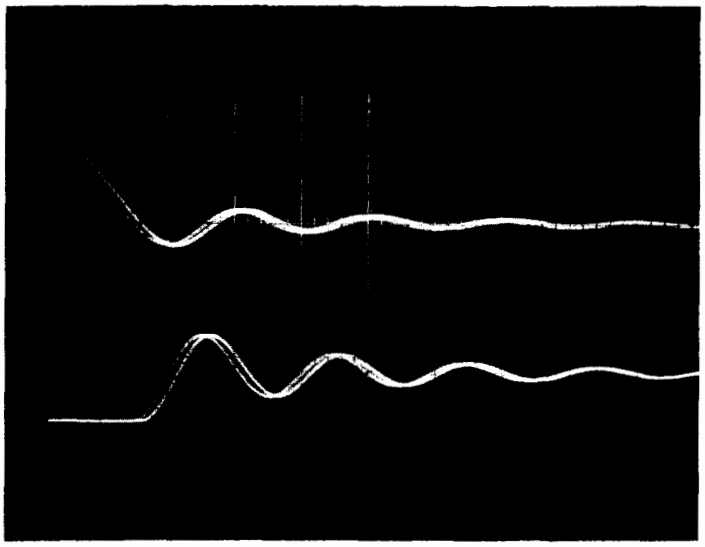

Fig. 19b--Some traces as above with a forward peak current of I_o = 120 amps.

Fig. 19--Oscilloscope pictures showing time dependence of positive ion current in a 5555 ignitron.

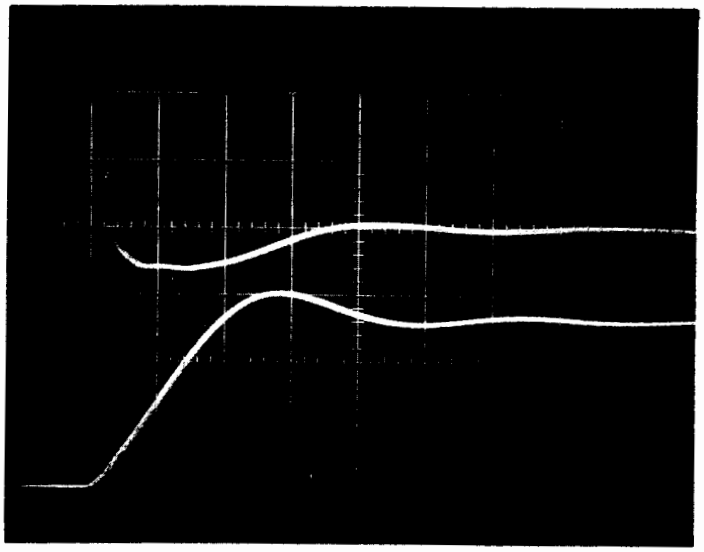

Fig. 20a--The top trace shows the ion-current vs time with the saturable reactor for the 5555 with a forward peak current value of I_o = 160 amps. The sensitivity is 1 amp/cm, and 10 μsec/cm. On the bottom trace the anode voltage wave form is shown where the sensitivity is 2 kV/cm and the speed is 10 μsec/cm. The repetition rate is R = 90 pps and T = 20.8°C.

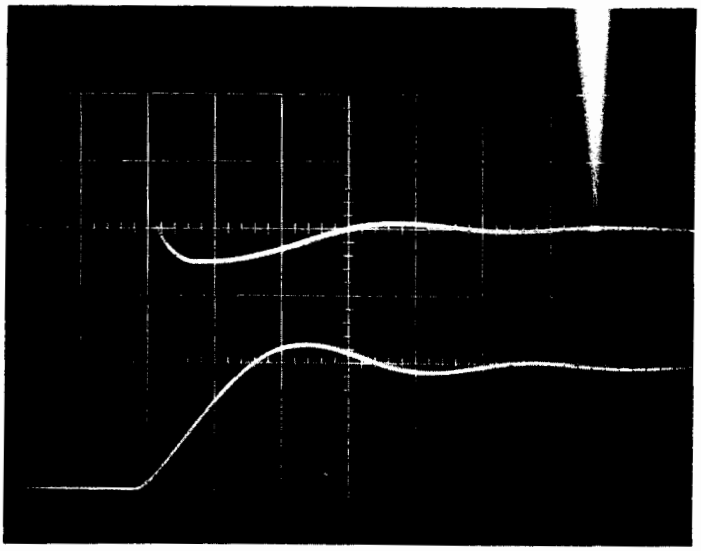

Fig. 20b--Some traces as above with a forward peak current of I_o = 120 amps.

Fig. 20--Oscilloscope pictures showing ion current of 5555 ignitron when saturable reactor is used to slow down the rate of voltage across tube.

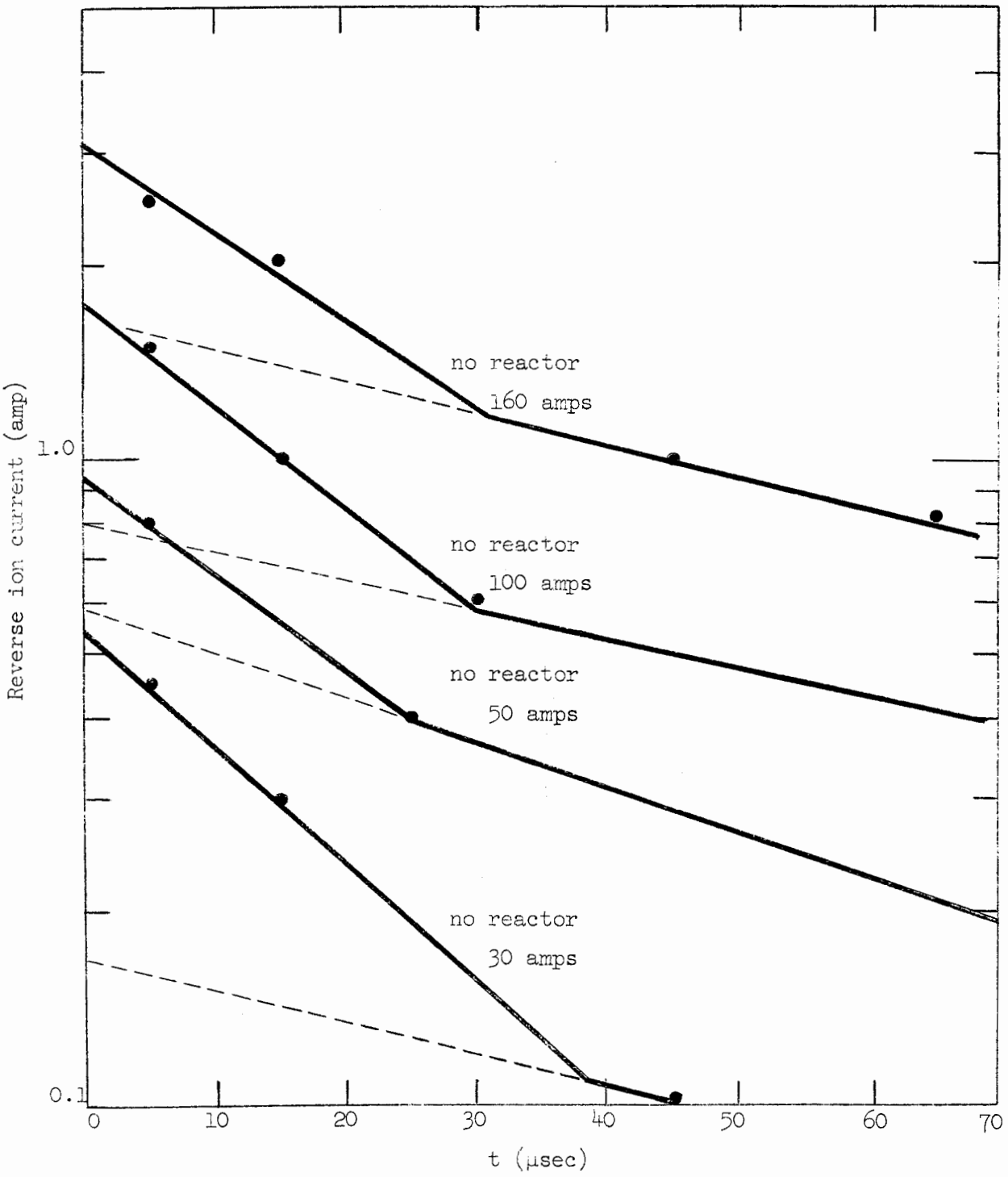

FIG. 21--Decay of the reverse ion current (current vs time).
Tube 5555;tube temperature 20.9°C.

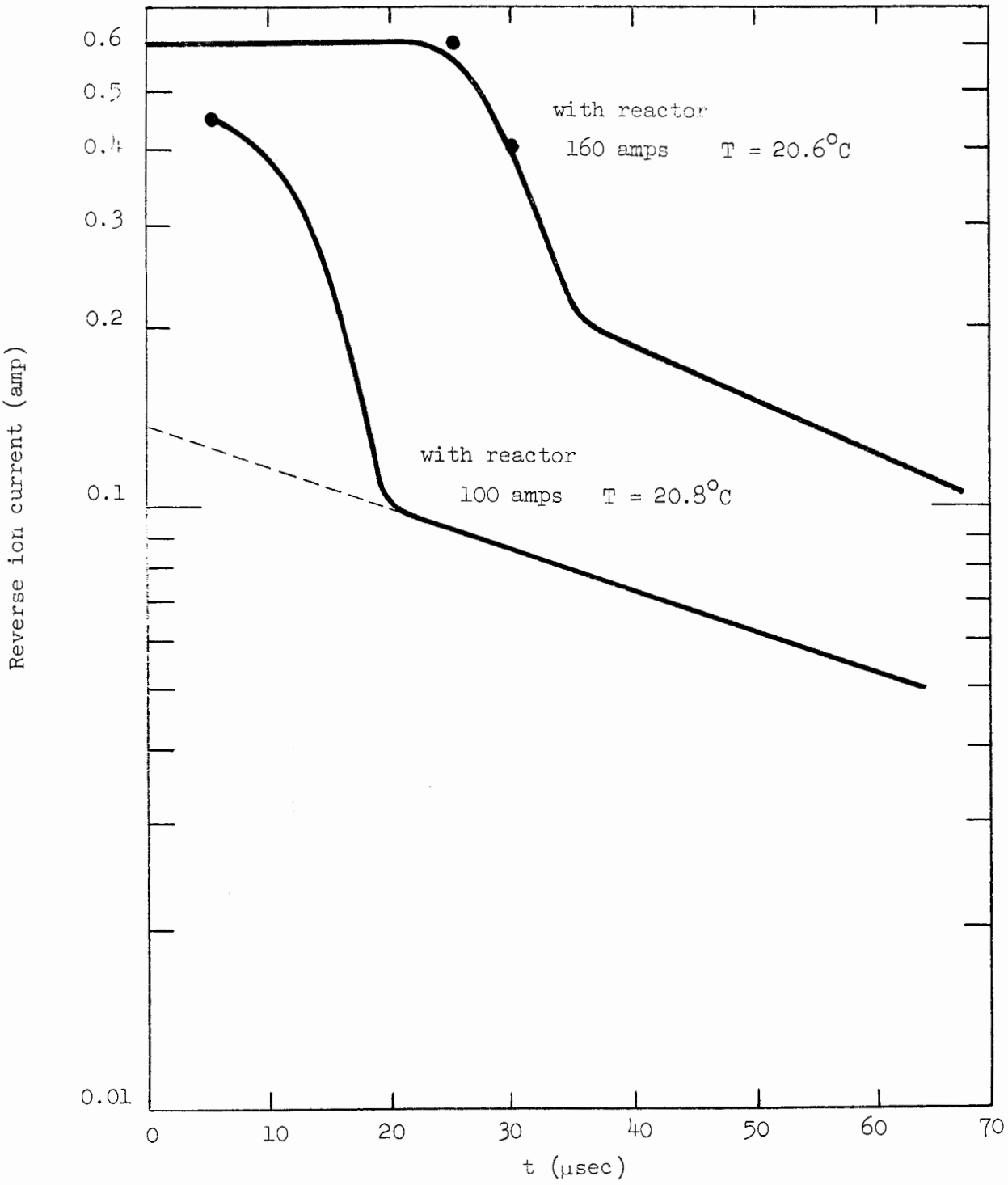

FIG. 22--Decay of the reverse ion current (current vs time).

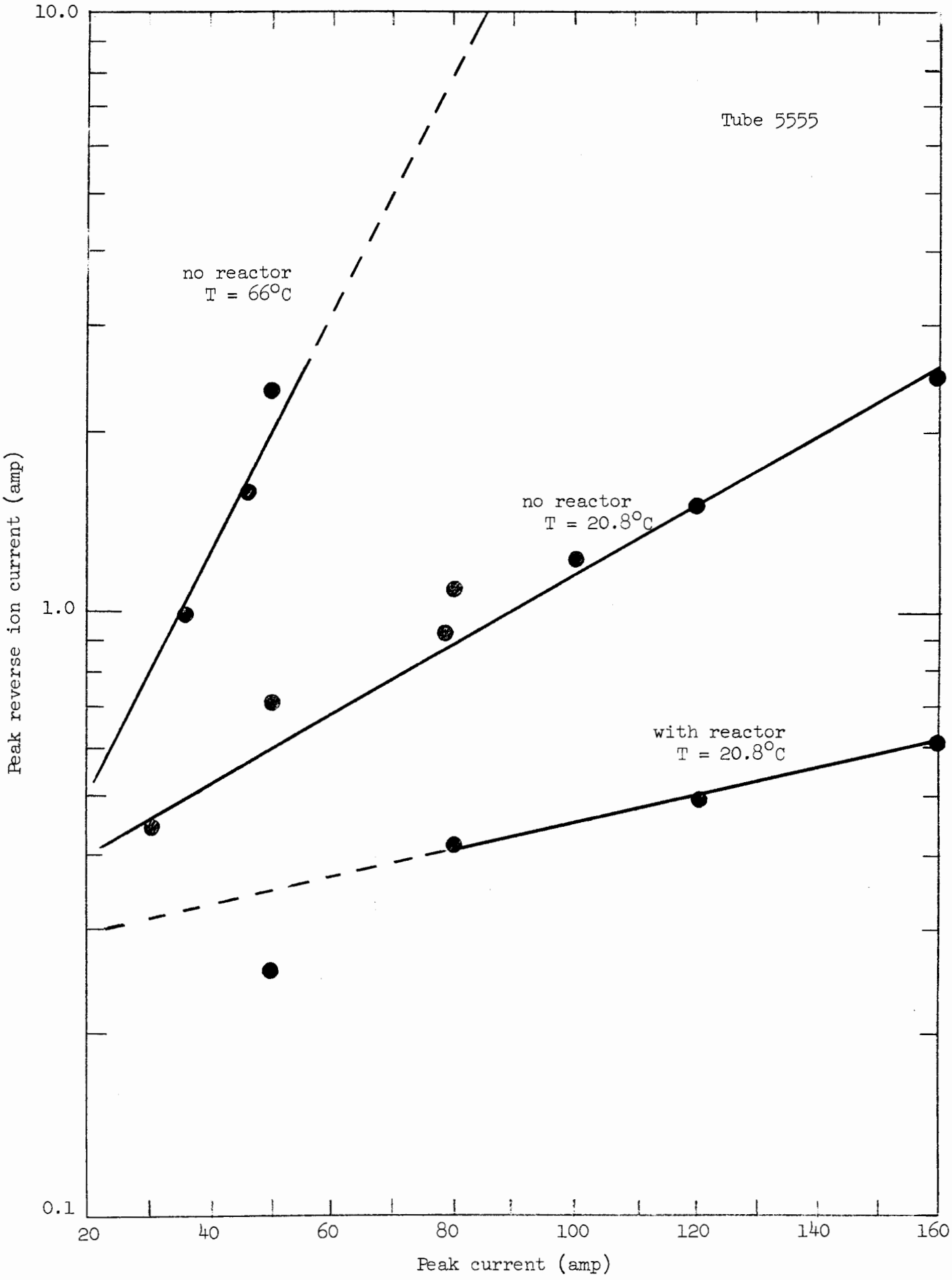

FIG. 23--Peak reverse ion current vs peak current.

deionization processes, which are the space-charge limited flow from the plasma to the anode with a time constant of $\tau_{conv} \approx 30$ μsec, and the diffusion current to the walls with $\tau_D \approx 30$ to 100 μsec. These currents are proportional to the charge density ($n_+ \approx n_-$) in the plasma, and because n_+ and n_- depend on the forward current (mostly electron current $j_-/j_+ \approx 600$), one would expect the peak ion current to increase with the forward peak current as shown in Fig. 23. The baffle or ring in the tube might eliminate a few forms of the possible cathode spot formation mechanisms and thus decrease the probability of the arcbacks; however, because the baffle does not prevent the ions from flowing to the negative "anode," the possibility of arcbacks still exists at high peak currents or long time constants (for example, a large diameter tube where $\tau_D \approx \frac{d^2p}{D_A}$ at high pressures, which in our interpretation might mean high repetition rate).

VII. INTERPRETATION AND GENERALIZATION OF THE KINGDON FACTOR

In the previous section it was mentioned that although the backstreaming ion current to the negative anode is the primary reason for reverse breakdowns, circuit parameters can also influence the probability of arcbacks. For example, circuit elements that minimize the Kingdon factor $V\left(\frac{dI}{dt}\right)$ reduce the arcback probability in a circuit in which the reverse voltage is applied immediately after the forward current pulse (see Fig. 24a). However, when the same negative voltage pulse is applied on the anode after the deionization time, the reverse breakdown would not occur because there are no ions in the tube (Fig. 24b). In this case, the Kingdon factor in the usual form $V\left(\frac{dI}{dt}\right)$ would not give correctly the conditions for arcback.

In this section we would like to show that it is possible to extend the basic idea of Kingdon and Lawton by demonstrating that the circuit elements which minimize the ion current also reduce the rate of arcbacks. As a special case it can be pointed out that this general formulation includes the familiar Kingdon factor as a measure of the arcback rate.

First, using a relatively simple model, one would like to relate the ion density $n_+ \approx n_-$ in the tube to the forward current. The forward

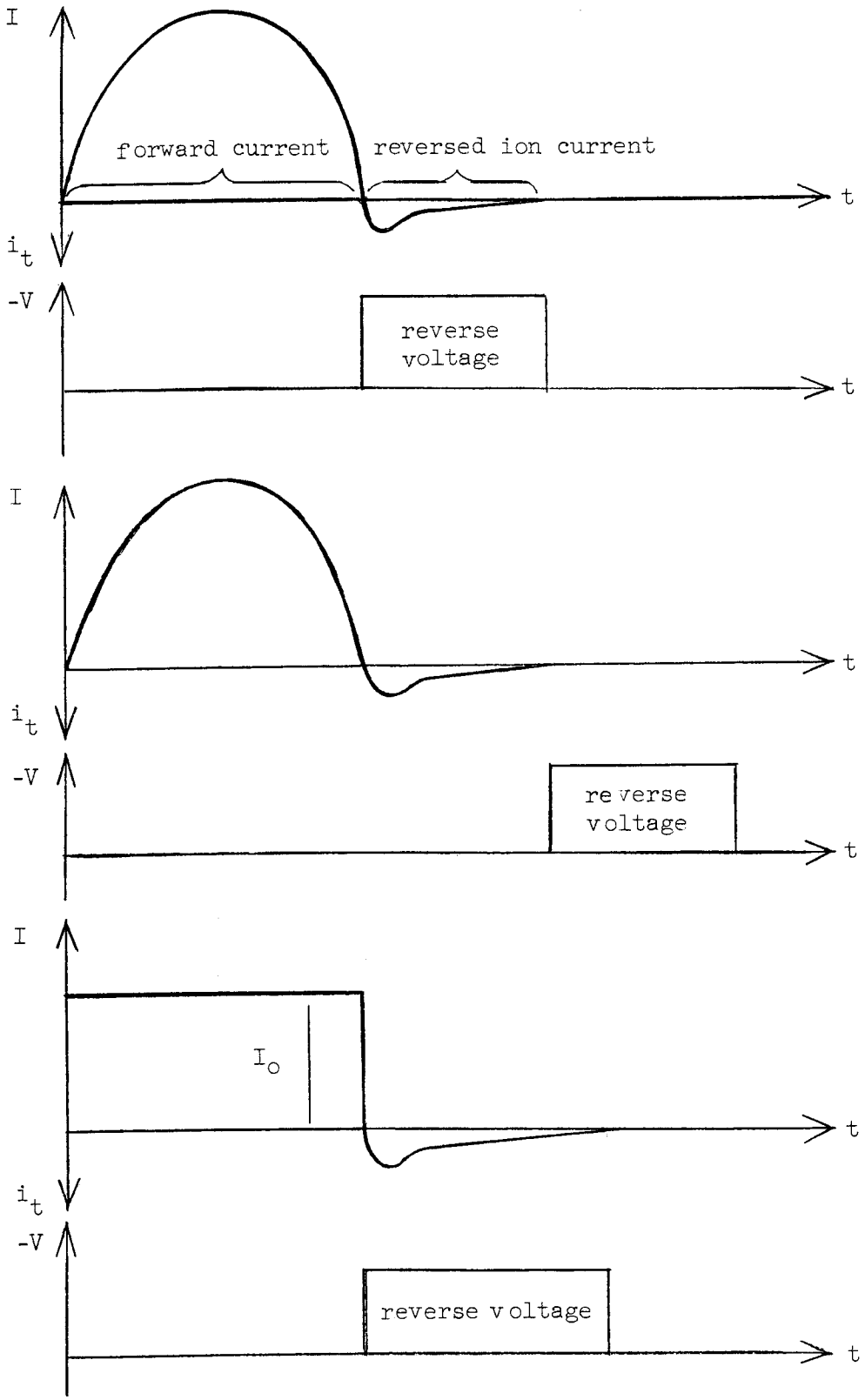

FIG. 24--Ignitron waveforms vs time.

current in the tube is carried primarily by the electrons; the total forward current density j can therefore be written approximately as

$$j = j_+ + j_- = j_-(1 + j_+/j_-) \approx j_-$$

because previous experiments have shown that $j_+/j_- \approx 1/600$. From the continuity equation then

$$e \frac{\partial n_+}{\partial t} = e \operatorname{div} j_-$$

but

$$e \frac{\partial}{\partial t} \int_{\substack{\text{tube} \\ \text{volume}}} n_+ dv = e \int_{\substack{\text{tube} \\ \text{volume}}} \operatorname{div} j_- dV = e \int_{\substack{\text{anode} \\ \text{surface}}} j_- df$$

after integration over time

$$en_+ = \frac{1}{V} \int_0^t \iint_{S_A} j_- df dt = \frac{1}{V} \int_0^t I(t) dt$$

and taking account of the ion diffusion current to the wall, one can write

$$en_+ \approx \frac{1}{V} \int_0^t I(t) e^{-t/\tau_{Diff}} dt$$

Using this formula at the end of the forward current pulse when $t = T$, the reverse current density to the negative anode can be calculated from

$$j_+(t) = \left[e \frac{D_A}{V_\ell} n_+ + en_+ \left(\bar{v}_+ + \frac{\delta h}{\delta t} \right) \right] e^{-\frac{t}{\tau_D}}$$

where

$$j_+(t) = \epsilon_o \left(\frac{8e}{m_+}\right)^{\frac{1}{2}} \frac{V^{3/2}(t)}{8h}$$

and

$$h(t) = \epsilon_o^{\frac{1}{2}} \left(\frac{8e}{m_+}\right)^{1/4} \frac{V^{3/4}(t)}{j_+(t)}$$

Hence

$$j_+(t) = en_+ f[V(t)] e^{-t/\tau_D}$$

Using these formulas, one can find the ion-density and with this the ion current density for different pulse shapes. For a square-wave forward current waveform with length T (Fig. 24c), using $\tau = \tau_{Diff}$ one gets

$$en^+ \approx \frac{1}{V} \int_o^T I_o e^{-t/\tau} dt = \frac{I_o \tau}{V} \left(1 - e^{-T/\tau}\right)$$

When $T/\tau \ll 1$,

$$en^+ \approx \frac{I_o T}{V}$$

and

$$j_+ \approx \frac{I_o T}{V} \left[\frac{D_A}{\Lambda_\ell} + \left(\overline{v}_+ + \frac{\delta h}{\delta t}\right)\right] e^{-\frac{t-T}{\tau_D}}$$

When $T/\tau \gg 1$,

$$en^+ \approx \frac{I_o \tau}{V}$$

and

$$j_+ \approx \frac{I_o \tau}{V} \left[\frac{D_A}{\Lambda_\ell} + \left(\bar{v}_+ + \frac{\delta h}{\delta t} \right) \right] e^{-\frac{t-T}{\tau_D}}$$

In the case of a half-sinusoidal pulse, with half-length T (Fig. 19a) and $I(t) = I_o \sin \frac{\pi}{T} t$, the ion density can be calculated as

$$en^+ \approx \frac{1}{V} \int_0^T I_o \sin \frac{\pi}{T} t \, e^{-t/\tau} \, dt = \frac{I_o e^{-t/\tau} \left(-\frac{1}{\tau} \sin \frac{\pi}{T} t - \frac{\pi}{T} \cos \frac{\pi}{T} t \right)}{V \left\{ (1/\tau)^2 + (\pi/T)^2 \right\}} \Bigg|_0^T =$$

$$= \frac{\frac{\pi}{T} e^{-t/\tau}}{V \left\{ (1/\tau)^2 + (\pi/t)^2 \right\}} \frac{dI(t)}{dt} \Bigg|_0^T$$

and the current density

$$j_+(t) \approx \frac{\pi/T e^{-t/\tau}}{V \left\{ (1/\tau)^2 + (\pi/T)^2 \right\}} \frac{dI(t)}{dt} \Bigg|_0^T f(V)$$

It can be seen that this expression for the positive ion current contains a term which is proportional to the product of the time derivative of the forward current at time T (end of the pulse) and a voltage dependent factor. This equation can, therefore, be considered a quantity which determines the rate of the arcbacks at the end of the forward current pulse. At a later time $t > T$, the current density proportional to the arcback rate is given as

$$j_+(t) \approx \frac{I_o \pi/T (e^{-T/\tau} + 1)}{V \left\{ (1/\tau)^2 + (\pi/T)^2 \right\}} \left[\frac{D_A}{\Lambda_\ell} + \left(\bar{v}_+ + \frac{\delta h}{\delta t} \right) \right] e^{-\frac{t-T}{\tau_D}}$$

which can be simplified when:

a) $T/\tau \ll 1$, then

$$j_+ \approx \frac{2I_o T}{V\pi}\left[\frac{D_A}{\Lambda_\ell} + \left(\bar{v}_+ + \frac{\delta h}{\delta t}\right)\right] e^{-\frac{t-T}{\tau_D}}$$

b) $T/\tau \gg 1$, then

$$j_+ \approx \frac{I_o \pi}{V}\left(\frac{\tau}{T}\right)\tau\left[\frac{D_A}{\Lambda_\ell} + \left(\bar{v}_+ + \frac{\delta h}{\delta t}\right)\right] e^{-\frac{t-T}{\tau_D}}$$

This formula gives a peak current density ($t = T$) of 0.1 amps/cm with $I_o = 160$ amps, $T = 0.5$ msec, $V = 10^3$ cm^3 and $\tau \approx 16$ μsec. This diffusion time-constant is smaller than the calculated diffusion time-constant ($\tau_D \approx 100$ μsec) after the forward pulse, which is not surprising because the effective pressure buildup during the pulse decreases D_A and thereby increases $\tau_{Diff} \approx \frac{1}{D_A}$.

It is obvious from this discussion that increasing the rise time of the negative anode voltage decreases the peak reverse current and that reducing the ringing of the inductor with the distributed capacitance of the coil will decrease the peak reverse voltage, and therefore decrease the arcback rate.

In the next section this theory will be applied to the operation of the gridded ignitron.

VIII. GRIDDED IGNITRONS

The conventional gridded ignitron consists of a sealed envelope which contains a mercury pool-cathode, ignitor electrodes, an anode, and one or more grids for various purposes. It is known that the operating temperature of a gridded ignitron is usually higher than for the gridless tubes. The reason for this is that the pressure is usually lower in the grid-anode region than between the cathode and the grid, and if the temperature is not high enough current limitation can occur. A simple interpretation of the current limitation can be given based on the

premise that the flux of positive ions to the tube walls cannot exceed the flux of neutral atoms into the grid-anode region. Despite the higher operating temperature and pressure the gridded tubes can hold a higher voltage because they have much smaller spacings between the electrodes than do the gridless tubes.

The probability of the arcbacks is usually small or non-existent in the gridded tubes. The reason for this is that the back-streaming ion current to the anode is decreased due to the fact that the negative grid helps in the deionization process, and the total number of ions in the grid-anode region is smaller because of the small volume. The ion current to the negative grid shows the same type of time dependence that was reported here earlier flowing to the negative anode. The ion current decays with two different time constants which are, according to H. S. Butler and T. F. Turner,[23] 15.7 μsec and 35.6 μsec.

Generally then, gridded tubes can be used when operating conditions exceed the usual 60 pps operation or when the timing of the tube firing is extremely critical.

Two gridded tubes were tested in the pulse magnet modulator: the GE 5630 which was designed for high voltage operation, and the GE 7736 which was designed for ≈2.5 kV operation. Both tubes were operated with no observed breakdown at full voltage (5 kV) and current (160 amps). Details about the operation of the prototype modulator using these tubes will be reported later.

IX. CONCLUSIONS

In this section the important conclusions of this ignitron-plasma study are summarized and the important parameters for the tube operation are given.

1. At high repetition rate operation it is possible to have a pressure build-up in the tube, which might be the primary reason for the forward breakdown.

2. The tubes with a built-in baffle break down easier in the forward direction than those that do not have a baffle. The reason for this is that the baffle helps in the transient-pressure build-up.

3. The transient pressure after the conduction cycle has a long time-constant 1 to 10 msec; the forward breakdown therefore can occur with decreasing probability 1 to 10 msec after the conduction cycle.

4. The most critical parameters influencing the rate of forward breakdown are the repetition rate and the temperature (R,T).

5. The deionization in a tube is controlled by the space charge-flow to the negative anode and by the ambipolar diffusion to the walls (τ_{conv} ~ 10 to 30 μsec, τ_{Diff} ~ 30 to 150 μsec).

6. The primary cause of the arcbacks is the ion-current flow to the anode.

7. The rate of arcbacks is proportional to the decaying ion current flow to the anode and therefore the breakdown probability is very high after the conduction cycle and decays exponentially thereafter.

8. By using external circuit elements to minimize the ion-current flowing to the negative anode it is possible to decrease the rate of arcbacks.

PLASMA PARAMETERS FOR THE IGNITRONS TESTED

	20°C	38°C	80°C
Neutral Density n_o	3.8×10^{13} cm^{-3}	1.6×10^{14} cm^{-3}	
Ion, Electron Density $n_+ \approx n_e$	$\sim 2.4 \times 10^{12}$ cm^{-3}	$\sim 4.8 \times 10^{12}$ cm^{-3}	$\sim 1.3 \times 10^{13}$ cm^{-3}
(mm pd Hg × cm)	1.1×10^{-2}	5×10^{-2}	9×10^{-1}
Breakdown Voltage	> 50 kV	~ 50 kV	~ 3 kV
Neutral Diffusion Time Constant		0.3 msec	6.8 msec
Neutral Mean Free Path		6.45×10^{-1} cm	2.82×10^{-2} cm
Thermalization Distance		< 6.45 cm	$< 2.82 \times 10^{-1}$ cm
Electron Temperature		23,000°K	10,000°K
Ambipolar Diffusion Time Constant $\tau_{Diff} = \frac{\Lambda^2}{D_A}$	30 μsec	115 μsec	4000 μsec
Time Constant for the Convection Ion-Flow τ_{conv}		30 μsec	
Debye Thickness		10^{-3} cm	

LIST OF REFERENCES

1. J. Slepian and L. R. Ludwig, Trans. AIEE 52, 692-8 (June 1933).
2. G. Mierdel, Wiss. Veröffentl. Siemens-Werken 15-16, 35 (1936-37).
3. E.G.F. Arnott, J. Appl. Phys. 12, 660-669 (1941).
4. W. W. Rigrod, J. Appl. Phys. 22, 787-796 (1951).
5. I. M. Tsinman, Radio Eng. and Electronic Physics No. 5., May 1963.
6. A. W. Hull, J. Appl. Phys. 35, 490 (1964).
7. L. Tonks, Phys. Rev. 48, 562-8 (1935).
8. J. R. Haynes, Phys. Rev. 73, 891 (1948).
9. G. Peche and W. Schmalenberg, Advances in Vacuum Science and Tech., Vol. II (1960), Pergamon Press.
10. H. C. Steiner, H. N. Price, Trans. AIEE 65 (1946).
11. L. B. Loeb, Kinetic Theory of Gases, Dover, Third Edition.
12. Engel-Steenbeck, Electrische Gasentladungen II (Springer, Berlin, 1934).
13. I. Langmuir and H. Mott-Smith, Gen. Elec. Rev. 27, 762 (1924).
14. T. J. Killian, Phys. Rev. 35, 1238 (1930).
15. B. Dosee-Mierdel, Der Elektrische Strom im Hochvackuum und in Gasen, (Hirzel, Leipzig, 1943).
16. J. E. Allen and P. C. Thonemann, Proc. Roy. Soc. 67, 768 (1954).
17. K. H. Kingdon, E. J. Lawton, Gen. Elec. Rev. 42, 474-8 (November 1939).
18. Wm. E. Pakala, C. J. Cucullu, AIEE Technical Paper 47-71 (December 1946).
19. J. E. Housley, G. N. Hughes, Trans. AIEE 65 (July 1946).
20. J. J. Muray, J. Appl. Phys. 33, 1525 (April 1962).
21. I. Langmuir and H. Mott-Smith, Gen. Elec. Rev 27, 538 (1924).
22. A. E. Robson, P. C. Thonemann, Proc. Phys. Soc. LXXIII, 508 (1959).
23. T. F. Turner and H. S. Butler, Proc. of the Seventh Symposium on Hydrogen Thyratrons and Modulators (May 1962).